POLITECNICO DI TORINO

Master's Degree in Biomedical Engineering

Master's Degree Thesis

New treatment for Duchenne muscular dystrophy based on zwitterionic polymers to encapsulate Adeno-Associated Virus vectors

Supervisors

Prof. Valentina Alice CAUDA

Prof. Marta GUERRA REBOLLO

Candidate

Chiara LEANDRO

March 2025

Motivations and Aims

Duchenne Muscular Dystrophy (DMD) is one of the most severe genetic disorders characterized by a progressive muscular degeneration affecting skeletal and cardiac muscles. It originates from mutations in the DMD gene, that is one of the largest known gene in the human body, and it affects the production of the protein dystrophin that is crucial for a correct functioning of the cytoskeleton.

Despite advances in supportive care, current treatments remain primarily symptomatic, and there is no definitive cure. The standard approach includes corticosteroid therapy, rehabilitation, and assisted ventilation, which have significantly improved the quality of life and extended life expectancy for patients by approximately 10 years. However, these treatments do not prevent the disease progression but slow only the process. This highlights an urgent need to explore innovative therapeutic approaches such as gene therapy, which offers the potential to fix directly the cause of the disease.
A novel strategy is to replace the faulty gene with a normal one, to modify the phenotype of the cell and restore the production of dystrophin. To deliver the therapeutic gene into the target cells viral vectors can be used, and the AAVs seems to be the most promising due to their low toxicity, high stability and long-lasting transgene expression.
But despite these advantages, there are also some limits. First, the size limitation of the genome has to be lower than 4,7 kb due to the low capacity of the vector. To overcome this, researchers developed a shortened gene called micro-dystrophin which is small enough to fit inside the vector.
Moreover, there is the problem of the host immune response [1].

This response includes neutralizing antibodies (nAbs) that are present in a large part of the population and can block the transgene delivery. Notably, approximately 70% of the population have NAbs for AAV1 and AAV2, 45% for AAV9 and AAV6, 38% for AAV8. In addition, many children affected with DMD have been exposed to AAV before, so they cannot participate in new trials in the future.
Therefore the challenge of the project is trying to decrease the AAVs recognition by the immune system by coating the viral vector but mantaining the natural tropism of the virus.

This master thesis highlights the importance of advancing research on AAV vectors for gene therapy, in line with the objectives of the Grup d'Enginyeria de Materials (GEMAT). The group initially attempted to coat AAVs with OM-pBAEs via electrostatic interactions, but the coating lacked stability, failing to protect AAVs from immune system clearance under physiological conditions. They then explored covalent binding using an NHS-functionalized pBAE, which proved effective in vitro but did not translate to successful in vivo results.

Therefore we want to investigate the use of click chemistry for covalently coating AAVs to overcome the limitations observed with the previous electrostatic and covalent approaches. The idea consists in covering the surface of the AAV with a zwitterionic polymer using click chemistry and comparing this strategy with the electrostatic one.

The strategy utilizing click chemistry involves two sequential reactions. The first reaction is the interaction between CliCr-Osu and the Adeno-associated virus (AAV), where CliCr-Osu chemically binds to the amines on the surface of the AAV. The second reaction occurs between the CliCr molecule, now attached to the AAV, and the polymer, resulting in the formation of a stable connection between the two components.

The first objective will be to characterize the CliCr-Osu compound to ensure its suitability as a functional linker and to understand its reactivity and compatibility with AAVs and polymers. Then transduction studies are conducted to investigate the intracellular trafficking of both coated and uncoated viral vectors. To establish a coating protocol, fluorescence-based analyses are performed to assess the initial reaction between CliCr-Osu and AAV and confirm that the AAV is properly prepared for subsequent conjugation with the polymer. A key aspect of the work involve comparing the stability of AAVs modified through the three distinct strategies: electrostatic interactions, covalent and linking enabled by click chemistry. This comparative analysis, is conducted through transduction studies and z-potential measure, to evaluate the advantages of click chemistry in terms of enhancing stability under physiological conditions. Finally, the coating's ability to target AAV to muscle cells is studied. This is achieved by testing different percentages of a zwitterionic polymer conjugated with a peptide and comparing the results to those obtained with unmodified (naked) AAVs.

To have an additional control, we synthesized a modified C6 pBAE polymer with an azide group on its lateral chain, which confers the ability to bind to the CliCr group. The resulting polymer is analysed and thermically characterized. Afterwards, once the synthesis of the modified polymer is performed, the resulting coated viral formulation is characterized.

Overall, this work advances the understanding of AAV entrance into cells and highlights the potential of the click chemistry to enhance the efficiency and safety of gene therapy for DMD patients.

Table of Contents

List of Tables

List of Figures

Acronyms

AAV

Adeno-Associated Virus

C6CR3

Arginine-terminated C6 pBAE

CliCr

CliCr®-Osu

Cy3

Cyanine 3

Cy5

Cyanine 5

DGC

Dystrophin-Glicoprotein Complex

DLS

Delayed Light Scattering

DMD

Duchenne Muscular Dystrophy

DMEM

Dulbecco's Modified Eagle Medium

DMSO

Dimethyl Sulfoxide

DNA

Deoxyribonucleic acid

DSC

Differential scanning calorimetry

FBS

Fetal Bovine Serum

FT-IR

Fourier transform infrared spectroscopy

GFP

Green Fluorescence Protein

ECM

Extra-Cellular Matrix

1H-NMR

Proton Nuclear Magnetic Resonance

HS

Horse Serum

MOI

Multiplicity of infection

NAbs

Neutral antibodies

NHS

N-hydroxysuccinimide

OM-pBAEs

Oligopeptide Modified pBAEs

pBAE

Poly(β-amino ester)

PBS

Phosphate Buffer Saline

pep2-zw

Zwitterionic polymer bonded with peptide 2

PFA

Paraformaldehyde

SPAAC

Strain Promoted Azide-Alkyne Cycloaddition

TGA

Thermogravimetric analysis

VP

Viral particles

Zw1

Zwitterionic polymer 1

Zw2

Zwitterionic polymer 2

Chapter 1

Introduction

1.1   Duchenne Muscular Dystrophy

Duchenne Muscular Dystrophy (DMD) is a rare, severe and progressive disease of skeletal muscle, respiratory insufficiency and cardiomyopathy. The word dystrophy comes from the Greek dys, which means "difficult", and troph, that means "nourish"[2]. The French neurologist Guillaume Benjamin Amand Duchenne was the first to describe the condition in the 1860s. However, it wasn't until the 1980s that significant progress was made in understanding the causes of muscular dystrophies. In 1987, Louis Kunkel identified dystrophin as the gene responsible of the desease[2].

It is one of the most common X-linked recessive disorders in human since it affect 1:5000 boys worldwide[3] [4].
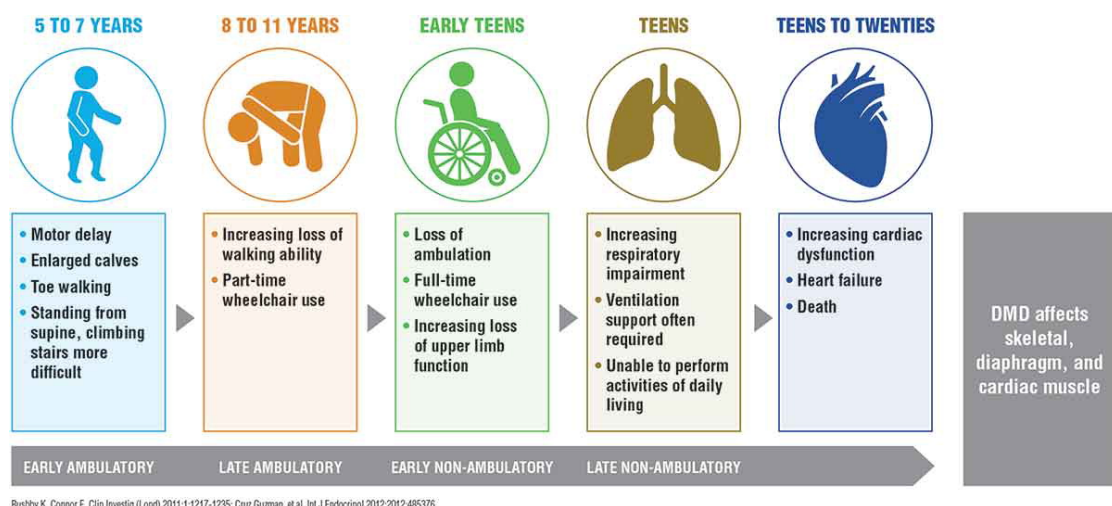
Figure 1.1: Progression of the disease

Children with DMD are usually diagnosed between ages 3 and 5 due to delays in early developmental milestones, such as sitting, walking, and talking. During this time, they may also have enlarged calf muscles, which are sometimes ignored or misunderstood[4]. By ages 5 to 7, more noticeable symptoms appear, such as difficulty standing and motor delays. As they grow older children lose the ability to walk, require a wheelchair, and in their teens and twenties start also the respiratory problems and heart issues due to a loss of diaphragm function. Ultimately, the disease leads to severe heart and lung failure, resulting in premature death[5].

It originates from mutations in the DMD gene that it is the largest known gene in the human body, so its mutation rate is quite high. More than 7000 different mutations have been identified, and they lead to an absence of production dystrophin, an essential cytoskeletal protein in muscle.

Dystrophin is a 427 kDa cytoskeletal protein essential to the Dystrophin-Glycoprotein Complex (DGC), a multi-protein structure that stabilizes muscle fibers by connecting the intracellular cytoskeleton to the extracellular matrix (ECM). This connection helps protect the sarcolemma from mechanical stress caused by muscle stretching and contraction. The DGC comprises Dystrophin, Dystroglycans, Sarcoglycans, Syntrophins, and Dystrobrevins, which collectively strengthen the muscle membrane and prevent contraction-induced damage.

Dystrophin itself consists of four main functional domains (**Figure 1.2**) [5] [3]:

1. N-terminal region that shares similarities with the actin-binding domains of α-actinin and serves to anchor dystrophin to the cytoskeleton;

2. Central rod domain composed of 24 spectrin-like repeats and four hinge regions that provides flexibility and structural support;

3. Cysteine-rich domain that connects dystrophin to the muscle membrane by interacting with the transmembrane protein β-Dystroglycan;

4. C-terminal domain that binds to α-Dystrobrevin and Syntrophins, facilitating the localization of dystrophin to the sarcolemma.
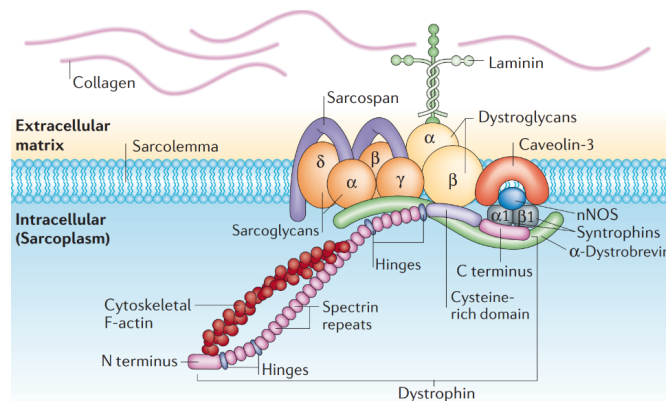
Figure 1.2: Schematic representation of Dystrophin (pink) and the Dystrophin-glycoprotein complex (DGC) including: Dystroglycans (yellow), Sarcoglycans (orange), Syntrophins (grey), Caveolins (red), Cytoskeletal F-actin (dark red) and more.

1.2 Current treatments

Currently, there is no curative treatment for DMD, but there are some strategies that can alter the natural course of the disease. Treatments can involve a combination of drug therapy, physical therapy, and surgery. Glucocorticosteroids, such as deflazacort or prednisone, are the current standard treatment and the most widely used therapy for patients with DMD. They can slow the rate of muscle deterioration by increasing overall muscle mass and strength. Nevertheless, these medicines have side effects and cannot be used for long-term. Other drugs that can be used are immunosuppressive drugs that can delay some damage to dying muscle cells, or antibiotics to treat respiratory infections. However, all these treatments only address the symptoms and do not target the underlying cause of the disease.

Physical therapy, which includes regular and moderate exercise, can help individuals maintain their range of motion and muscle strength. This approach can prevent deformities, enhance movement, and keep muscles as flexible and strong as possible. However, the combination of steroid treatments and low levels of daily physical activity often leads to excessive weight gain in infants, which can affect mobility and increase the risk of complications such as skeletal fractures. To reduce these risks, maintaining a well-balanced diet is crucial. Furthermore, calcium and vitamin D supplementation is recommended to support bone health, prevent fractures, and counteract deficiencies resulting from limited sunlight exposure[6].

Finally, also corrective surgery can be used to ease complications from DMD and reduce the pain[2].

1.2.1 Gene Theraphy

Since DMD is caused by several mutations in a single gene, gene therapy is a promising way to treat it. It is a technique that consists in modulating the gene expression by transferring genetic material directly in specific cells of a patient to treat or cure disease and can work by several mechanisms[7].

The **gene addition**, addresses more complex diseases, such as autoimmune or infectious conditions, by incorporating new genetic material into cells without replacing the existing, malfunctioning genes. This technique is used in the ongoing AAV-based therapies for rheumatoid arthritis, where a single injection can provide localized and regulated anti-inflammatory effects. Duchenne Muscular Dystrophy (DMD) gene therapy also falls under this category, as current treatments introduce a micro-dystrophin or mini-dystrophin gene using AAV vectors to restore partial dystrophin function without replacing the entire faulty gene[8].

The second strategy, the **gene silecing** uses RNA interference (RNAi) to silence harmful gene expressions caused by gain-of-function mutations. AAV vectors are employed to deliver microRNA precursors targeting specific mRNA sequences. An example is the use of AAV in Huntington's disease to reduce the expression of the mutant huntingtin protein, addressing the underlying cause of the disease.

Finally, the **gene replacement** works by replacing the faulty gene in affected cells to address the root cause of the disease. The idea is that by substituting the mutated gene with a healthy one, the disease could potentially be cured. This approach is exemplified by therapies for disorders like severe combined immunodeficiency (SCID), where a functional copy of the defective gene is delivered to patient cells.

Successful cases in recent years have shown that gene therapies can provide long-term health benefits, inspiring hope and efforts to make these therapies part of standard treatments.

To deliver the therapeutic gene into the target cells, gene therapy can use a carrier known as a vector. An ideal vector should precisely target the intended cells for transfection, effectively encapsulate and protect the genetic material, and ensure long-term gene expression. Engineered vectors are generally categorized into viral and non-viral types.

Since the beginning of the gene therapy, **non-viral vectors** have gained considerable attention due to their lower pathogenicity, reduced immunotoxicity, cost-effectiveness, and ease of production compared to viral methods. They come in various forms, broadly classified into inorganic particles, lipid-based carriers, and polymer-based carriers[9]:

- Inorganic particles, such as gold nanoparticles or calcium phosphate, facilitate gene delivery through their stability and ease of modification.

- Lipid-based carriers, including liposomes and lipid nanoparticles, enhance

cellular uptake by mimicking biological membranes.

- Polymer-based carriers, like polyethyleneimine (PEI) and chitosan, offer tunable properties for efficient gene encapsulation and controlled release.

Despite the wide variety of non-viral vectors available, their transduction efficiency remains low, and transgene expression is often weak and short-lived. As a result, non-viral vectors are used in less than 25% of clinical trials. For Duchenne muscular dystrophy (DMD) treatments, viral vectors are the preferred choice due to their natural ability to infect cells and efficiently deliver genetic material to target tissues[10].

1.3 Viral Vectors

Viral-mediated gene therapy holds great promise for treating Duchenne Muscular Dystrophy (DMD) by aiming to restore dystrophin production. This approach has the potential to benefit all DMD patients, regardless of their specific dystrophin mutation. Common types of viral vectors include Adenovirus, Retrovirus, Lentivirus, and Adeno-Associated Virus (AAV) and we can see a comparison in Table 1.1[11]. In the **Figure 1.3** the various types of viral vectors.
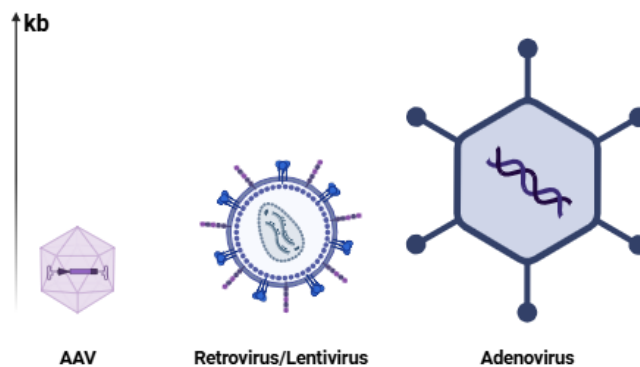
Figure 1.3: Viral vector types arranged in increasing order of package size

1.3.1 Adenovirus

Adenoviruses are large non-enveloped viruses belonging to the Adenoviridae family. First isolated in 1953 by Wallace Rowe, adenoviruses have an intricate icosahedral capsid that protects a 36 kb double-stranded DNA genome. Over 50 adenoviral serotypes exist, but the most commonly used for gene therapy are human serotypes

Characteristic	Adenovirus	Retrovirus	Lentivirus	AAV
Family	Adenoviridae	Retroviridae	Retroviridae	Parvoviridae
Viral genome	dsDNA	ssRNA	ssRNA	ssDNA
Package size	30 kb kb	9 kb	9 kb	<5
Cell transduction	Dividing and non-dividing	Dividing	Dividing and non-dividing	Dividing and non-dividing
Integration to host's genome	No	Yes	Yes	Yes (specific site)/No (episome)

Table 1.1: Comparison of Viral Vectors

Ad2 and Ad5. Adenoviruses are valuable tools in gene therapy due to their generally self-limiting and non-fatal infections, and they have been used in over 500 clinical trials. Their ability to infect both dividing and non-dividing cells makes them versatile for gene delivery. In gene therapy, up to 30 kb of the adenoviral genome can be replaced with foreign DNA.

Adenoviruses are particularly effective because they can transduce a wide range of cells. However, their lack of full integration into the host genome means that gene expression is typically transient, with the transgene often being lost within days post-transduction. Despite this limitation, adenoviruses remain an important vector for gene therapy, particularly in applications where high but temporary gene expression is needed[12][9].

1.3.2 Retrovirus

Retroviruses are a group of single-stranded RNA viruses that are characterized by their ability to reverse transcribe their RNA genome into DNA inside a host cell. This process is carried out by the enzyme reverse **transcriptase**. Once the RNA is converted into DNA, it is integrated into the host cell's genome, where it can remain as a part of the host's DNA. Retroviruses are typically lipid-enveloped and have a relatively simple structure, with an RNA genome of approximately 10 kilobases. They are particularly useful for gene therapy in proliferating cells but require the host cell to be actively dividing for integration to occur. However, retrovirus vectors also pose a risk of insertional mutagenesis, which can lead to unintended genetic changes or activation of oncogenes[9].

1.3.3 Lentivirus

Lentiviral vectors (LV), derived from the human immunodeficiency virus (HIV), have been used in over 270 clinical trials since the mid-1990s. Belonging to

the Retroviridae family, LV are lipid-enveloped, spherical particles with a single-stranded RNA genome of around 10 kb, which is converted into double-stranded DNA during replication. LV are efficient gene transfer vectors for both dividing and non-dividing cells. Once inside a cell, the RNA genome is reverse transcribed into proviral DNA, which forms a preintegration complex (PIC) that is imported into the nucleus. The provirus is integrated into the host genome, enabling permanent gene expression.

1.3.4 Adeno-Associated Virus

Biology of AAV
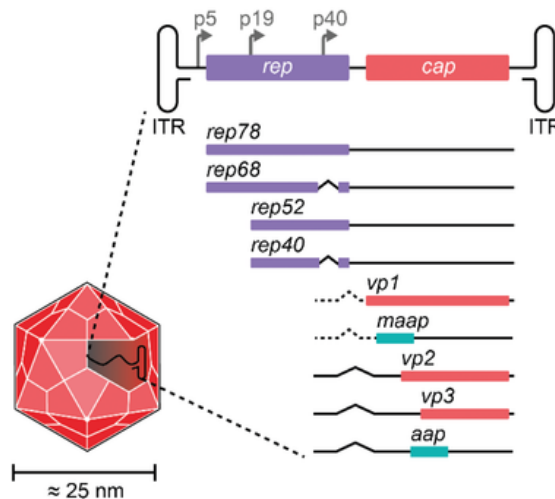
Figure 1.4: Genomic organization of AAV

AAV is a single-stranded DNA Parvovirus with a 4,7 kb genome that includes four known parts, rep, cap, MAAP and AAP, accompanied by two 145 bp Inverted Terminal Repeats (ITRs)(**Figure 1.4**). ITRs are structural elements required for second strand synthesis, genome amplification, integration into the chromosome, and ssDNA packaging.

The **rep gene** controls viral replication and integration, and encodes four non-structural proteins of different molecular weight (Rep40, Rep52, Rep68, Rep78). They are produced from two alternatively spliced mRNAs whose expression is controlled by the two promoters p5 and p19. The **cap gene** encodes three viral proteins, VP1,VP2 and VP3 that form the icosahedral capsid with a size of 23-28 nm. These proteins are produced in a 1:1:10 ratio (VP1:VP2:VP3) and are produced from the alternative splicing from the P40 promoter. Finally, there are

the membrane-associated accessory protein (**MAAP**) and the assembly-activating protein (**AAP**).

AAVs are capable of transducing both dividing and non-dividing cells, making them versatile for therapeutic applications.

Tropism

There are at least 12 known serotypes of AAVs, depending on their capsid proteins, that bind to different specific surface receptors. The most common are AAV1-AAV9, and they have different tissue tropism (**Table 1.2**). In particular, the the AAV2 is the most used and studied in gene therapy. The serotypes AAV1, AAV6, AAV7, AAV8, and AAV9 have the ability to efficiently target striated muscles, which include skeletal muscle and cardiac muscle.

Serotype	Tissue Tropism	Applications
AAV1	Muscle, Heart	Muscular dystrophy, gene therapy
AAV2	Liver, Muscle, CNS	Liver, muscle, and CNS disorders
AAV5	Lung, Liver, CNS	Lung and liver diseases, CNS disorders
AAV6	Muscle, Liver	Muscle-targeted gene therapy
AAV8	Liver, Muscle	Liver-targeted gene therapy, muscle
AAV9	Muscle, Heart, CNS	CNS disorders, muscle diseases, heart
AAV4	Lung, CNS	Lung and CNS-targeted gene therapies
AAV3	Liver	Liver-targeted gene therapy
AAV-DJ	Liver, Muscle, CNS	Broad applications, hybrid for multiple organs
AAVrh10	Liver, CNS	Liver and CNS gene therapies
AAV7	Liver, Muscle	Liver-targeted therapies
AAV12	Similar to AAV9	Experimental use for gene therapy

Table 1.2: Comparison of AAV Serotypes

Infection cycle

AAVs do not replicate independently, but require a helper virus for their lifecycle, such as an adenovirus or herpes simplex virus.

They enter in the cells through a multi-step process (**figure 1.5**). After binding to cellular receptors, AAV is internalized via endocytosis. Endosomal acidification triggers conformational changes in the capsid, exposing the phospholipase A2 (PLA2) domain. The virus then traffics through the Golgi apparatus and escapes into the cytoplasm before entering the nucleus through the nuclear pore complex. Inside the nucleus, the AAV genome is uncoated and converted into double-stranded DNA, leading to three possible outcomes [13][11]:
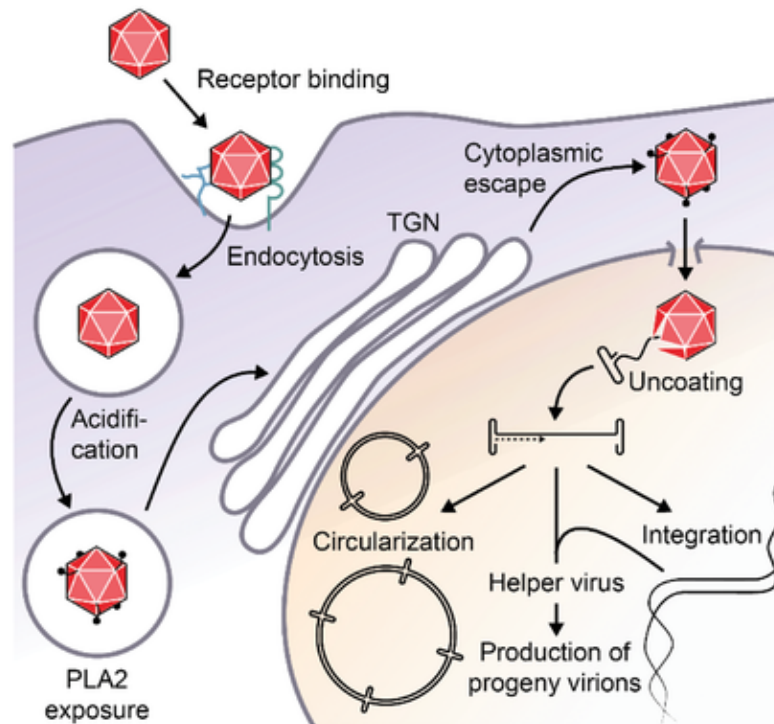
Figure 1.5: Mechanisms of internalization of AAVs

1. In the absence of helper functions, the genome integrates into the host DNA, establishing a latent infection

2. With a helper virus, AAV undergoes replication and produces progeny virions

3. Recombinant AAV (rAAV), which lacks Rep proteins, ensures long-term transgene expression through circularization and the formation of high-molecular-weight concatemers

Advantages and Disadvantages

The AAVs offer several advantages for gene therapies, but present also some limitations.
One of the greatest benefits is that AAVs are **non-pathogenic** and elicit a relatively low immune response compared to other viral vectors. Their episomal genomes can persist for years in non-dividing cells, enabling **long-term gene expression** while minimizing the risk of insertional mutagenesis due to their **low genomic integration rate**. Additionally, AAV vectors have broad tissue tropism, so they can efficiently target various tissues depending on their capsid proteins. Their small

size also allows them to cross biological barriers, such as the blood-brain barrier.

However, AAVs also have some limitations. Due to their small size, they have a limited cargo capacity (<5kb). Moreover, there is the problem of the host immune response[1]. This response includes neutralizing antibodies (nAbs) that are present in a large part of the population and can block the transgene delivery. Notably, approximately 70% of the population have NAbs for AAV1 and AAV2, 45% for AAV9 and AAV6, 38% for AAV8. As a result, many children affected by DMD may have been previously exposed to AAVs, preventing them from participating in future clinical trials.

Therefore, the two primary challenges are the large size of the dystrophin gene and the need to shield the AAV from the immune system without loosing the natural tropism of the virus[14].

1.4 Engineering of the AAVs

To address the limitations of AAVs discussed earlier, extensive efforts have been made to engineer AAV vectors with enhanced functionality. Strategies such as capsid modification, the development of novel serotypes with reduced immunogenicity, and genome optimization techniques have been explored to enhance transgene packaging and evade immune responses. This chapter will discuss these advances in AAV engineering, focusing on how they contribute to overcoming current limitations and expanding the potential of AAV-based gene therapies.

Small size

The enormous size of the dystrophin gene poses a major challenge for using recombinant AAV (rAAV) as a delivery system for DMD gene therapy, given that AAV's maximal packaging capacity is around 4.7 kb. To overcome this limitation, researchers have developed truncated versions of the dystrophin gene that retain essential functional domains while fitting within the AAV vector (**figure 1.6**). Two primary classes of abbreviated dystrophin genes exist[15]:

1. **mini-dystrophin**, which ranges from 6 to 8 kb and contains more than four spectrin repeats (SRs)

2. **micro-dystrophin**, which is approximately 3.5 to 4 kb and has four or fewer SRs

Since the size of mini-dystrophin exceeds AAV's packaging limit, micro-dystrophin| is the preferred option for gene therapy applications.

A critical question in DMD therapy is whether micro-dystrophin can provide sufficient functional benefits to patients. Preclinical studies have demonstrated that rAAV-mediated delivery of optimized micro-dystrophin constructs can significantly improve muscle pathology, enhance muscle force, and restore cardiac function in animal models of DMD.

These findings support the potential of micro-dystrophin gene therapy as a viable treatment strategy for DMD, paving the way for clinical trials aimed at assessing its efficacy and safety in human patients.
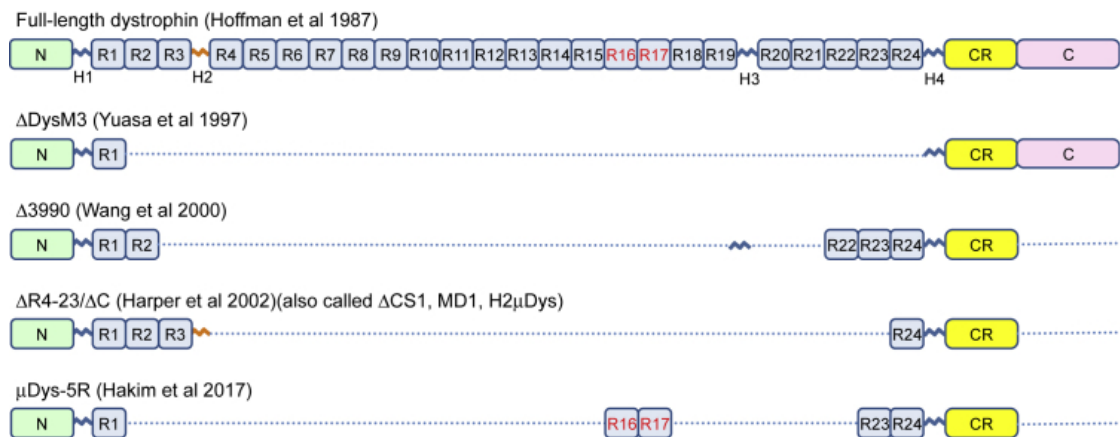
Figure 1.6: Full-length dystrophin consists of an N-terminal domain (N), 24 spectrin-like repeats (R1 to R24), four hinges (H1 to H4), a cysteine-rich domain (CR), and a C-terminal domain (CT). In contrast, micro-dystrophins, which have been synthesized over the past 20 years, are truncated versions of dystrophin that retain only key functional domains

11

Immune recognition
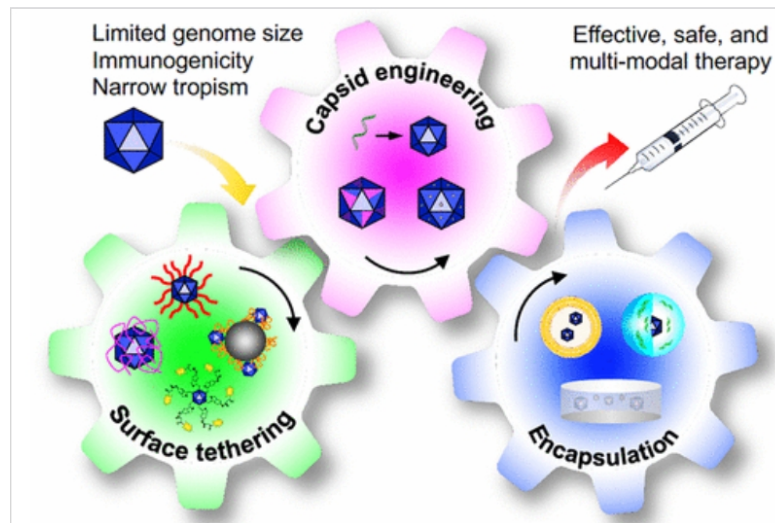
Figure 1.7: Strategies for enginering AAVs

Several strategies have been developed to enhance AAV's therapeutic potential and escape from the immune recognition (**figure 1.7**).

Capsid engineering has emerged as a pivotal approach, involving modifications to the virus's protein shell to improve functionality, tissue targeting, and immune evasion. One method, the creation of chimeric capsids, integrates genetic elements from multiple serotypes, allowing for enhanced tissue specificity and evasion of neutralizing antibodies (nAbs). Similarly, mosaic capsids combine capsid proteins from different serotypes, expanding targeting capabilities and reducing recognition by pre-existing antibodies. Finally, transcapsidation involves packaging the genome of one serotype into the capsid of another.

Surface tethering represents another transformative strategy to enhance the functionality of the AAV. By attaching polymers such as polyethylene glycol (PEG) or poly-beta amino esters (pBAEs) to the virus's capsid, immune recognition is minimized, and circulation time in the bloodstream is extended. Additionally, the virus's anionic charge of -11 mV allows for complexation with cationic polymers. Lysine residues with available primary amines on the AAV surface allow for facile conjugation with desired molecules via EDC/NHS coupling. However, an excessive amount of polymer can interfere with cellular uptake and reduce transduction efficiency. Beyond polymers, ligands and imaging probes can be conjugated to AAV capsids, enabling precise targeting of specific receptors and facilitating in vivo visualization.

Encapsulation offers additional opportunities to refine AAV delivery. Enclosing AAVs in carriers such as liposomes, hydrogels, or extracellular vesicles protects them from immune responses while enabling stimuli-responsive delivery. These carriers can also be integrated into large-scale biomaterial platforms, enhancing their therapeutic versatility. Through these advanced strategies, AAV's safety, efficacy, and versatility as a gene therapy tool are significantly enhanced[16].

1.4.1   Polymer coating

A promising strategy to improve the efficiency of viral vector delivery and immune evasion during systemic administration is the development of hybrid vectors. By coating AAVs with polymers, the viral capsid can be shielded from undesirable interactions with the biological environment. These hybrid vectors are expected to offer improved cellular binding, uptake, endosomal escape, and nuclear delivery of genetic material, making them a valuable innovation in gene therapy.

In particular, this project concentrates on the use of zwitterionic polymers and pBAEs to create a hybrid vector with AAV.

pBAEs

Poly(β-amino ester)s are a class of biodegradable cationic polymers first synthetized in the 1980s and intensively studied since the 2000s for their potential in gene delivery. PBAEs are linear or branched polymers composed of repeating β-amino ester units. These units are formed by combining amines and diacrylates through a Michael addition reaction[17]. The resulting polymers have ester bonds in their backbone, which make them hydrolytically degradable. The key characteristics of this class of polymers are [18] [17]:

- **Biodegradability**: The ester bonds in the backbone hydrolyze under physiological conditions, producing non-toxic byproducts.

- **pH Responsiveness**: The tertiary amines in pBAEs contribute to a "proton sponge effect," facilitating endosomal escape for intracellular delivery.

- **Low Toxicity**: Compared to other cationic polymers like polyethyleneimine (PEI), pBAEs have a lower surface charge density, reducing cytotoxicity while maintaining high transfection efficiency.

- **Structural Diversity**: pBAEs can be tailored through various monomer combinations, reaction conditions, and end-group modifications to optimize their physicochemical properties for specific applications.

The general structure of PBAEs consists of two main components: the **diacrylate monomer** that provides the ester backbone, and the **amine monomer** that
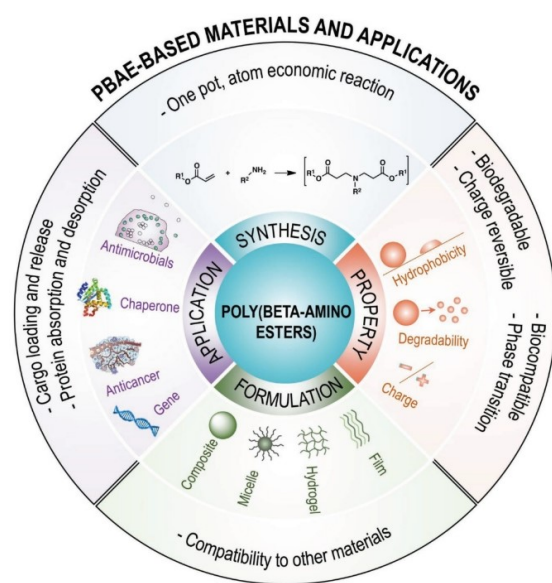
Figure 1.8: Schematic summary of pBAEs-based materials and applications

allows for further customization and functionalizations. Changing the R' chain, we can tune the characteristics of the polymer (**figure 1.9**).
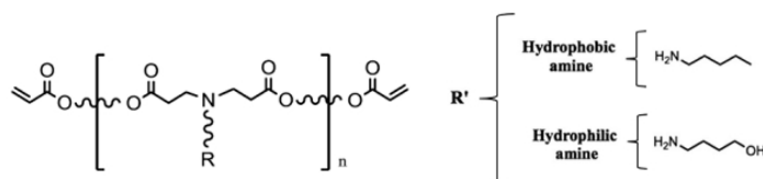
Figure 1.9: pBAEs chemical structure

Oligopeptide end-modified pBAES: OM-pBAEs

The GEMAT group has developed a family of oligopeptide-terminated pBAEs for gene delivery (figure 1.10), inspired by natural polypeptide-based vectors. These oligopeptides enhance gene transfection efficiency by improving interactions between pBAE/DNA nanocomposites and target cells in a cell-type-specific manner. Among them, arginine-rich oligopeptides, with their strong positive charge, exhibit the highest transfection efficiency[19].

Previous studies, demonstrated that oligopeptide-modified pBAEs are highly effective as non-viral gene delivery vectors, offering excellent transfection efficiency, biocompatibility, and cell specificity both in vitro and in vivo[20][21]. Hybrid vectors
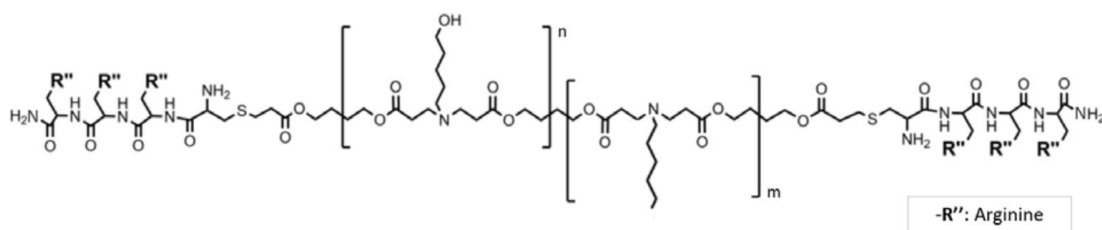
Figure 1.10: Chemical structure of oligopeptide end-modified pBAE (OM-pBAE)

combining pBAE and AAV were developed for gene therapy to treat Duchenne muscular dystrophy (DMD). These vectors relied on electrostatic interactions between the negatively charged AAV capsid and the positively charged arginine-rich pBAEs. However, during in vivo experiments, the polymer coating proved unstable, necessitating the development of a more stable alternative.

Therefore, a covalent coating approach was explored to enhance the stability of pBAE-AAV interactions. The hydrophilic amine side chain of the C6-50 pBAE was modified with an N-hydroxysuccinimide (NHS) acid derivative to enable covalent bonding with AAV capsid proteins, ensuring stronger and more durable interaction. Additionally, CR3 peptides were attached to the acrylate groups of the polymer to further improve its properties and functionality (**figure 1.11**).
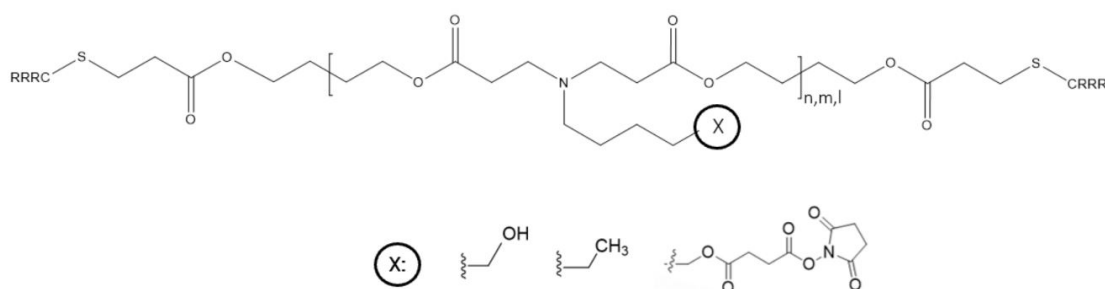
Figure 1.11: Chemical structure of the modified OM-pBAE: C6 one-acid activated pBAE with CR3 peptides

To address the limitations observed with the previous approaches, we propose investigating the application of click chemistry as an alternative strategy for coating AAVs. This approach seeks to address the limitations of electrostatic coatings, including instability and unpredictability, while also overcoming the constraints of the covalent strategy by enabling more precise and stable surface modifications.

We will then compare the performance of this click chemistry-based coating with the traditional electrostatic method to evaluate improvements in coating efficiency, stability, and overall effectiveness.

Zwitterionic polymers

Zwitterionic polymers are a unique class of macromolecules that contain both positively and negatively charged functional groups within the same repeating unit, resulting in an overall net neutral charge. These polymers have gained significant interest in biomedical and material science applications due to their excellent antifouling properties, high hydration capacity, and biocompatibility[22]. These characteristics enable zwitterionic nanocarriers to evade the reticulo endothelial system (RES), the body's primary mechanism for clearing foreign particles from the bloodstream, leading to prolonged circulation times.

Zwitterionic polymers can be broadly categorized into:

- **polybetaines**: such as polysulfobetaine (PSB), polycarboxybetaine (PCB), and phosphorylcholine (PC) polymers

- **mixed-charge zwitterionics**

Their versatility allows for precise tailoring to suit various biomedical applications, depending on their molecular structure and specific properties.

The distinctive feature of zwitterionic polymers is their simultaneous presence of cationic and anionic groups, which result in an overall neutral charge. Common cationic groups include quaternary ammonium and pyridine, while anionic groups often consist of carboxylate, sulfonate, or phosphate (**figure 1.12**). This balanced charge distribution leads to a high dipole moment, facilitating strong hydration and electrostatic stability[23].

Figure 1.12: Common cationic and anionic groups in zwitterionic polymers

1.4.2 Peptide-Mediated Targeting in Duchenne Muscular Dystrophy

This thesis investigates muscle-specific peptide targeting to enhance AAV-based delivery systems for Duchenne Muscular Dystrophy (DMD) and other muscular disorders. Several peptides have been identified for their specificity toward muscle cells, making them promising candidates for therapeutic applications. By attaching these peptides to AAV vectors, precise delivery of therapeutic nucleic acids can be achieved directly to dystrophic myotubes, improving therapeutic efficacy while minimizing side effects. Additionally, the effects of these peptides are studied in relation to both zwitterionic and pBAE polymers, providing insights into their interactions and potential for optimized delivery.

One peptide, RGDLGSC (AAVMYO), was extensively studied for its effectiveness and selectivity toward muscle cells[24]. This peptide interacts with the $\alpha7\beta1$ integrin, a receptor important for muscle cell regeneration. The $\alpha7\beta1$ integrin links the basal lamina and muscle fibers, crucial for muscle function and repair[25]. Increased expression of the $\alpha7$ integrin is observed in DMD patients and mdx mice, making this peptide particularly relevant for targeted therapy in DMD.

17

1.5 Click chemistry

The term "Click Chemistry" was used for the first time in the 1999 by K. B. Sharpless to define a series of reactions that are fast, efficient, and produce high yields with minimal by-products[26]. These reactions are simple to perform, require mild reaction conditions, and are highly selective. The idea is that the reagents "click" together in a predictable way, like pieces of a puzzle[27].

These characteristics make them ideal for applications like bioconjugation, a method that forms a stable bond between two molecules, with at least one being a biomolecule or one of its derivative[28].
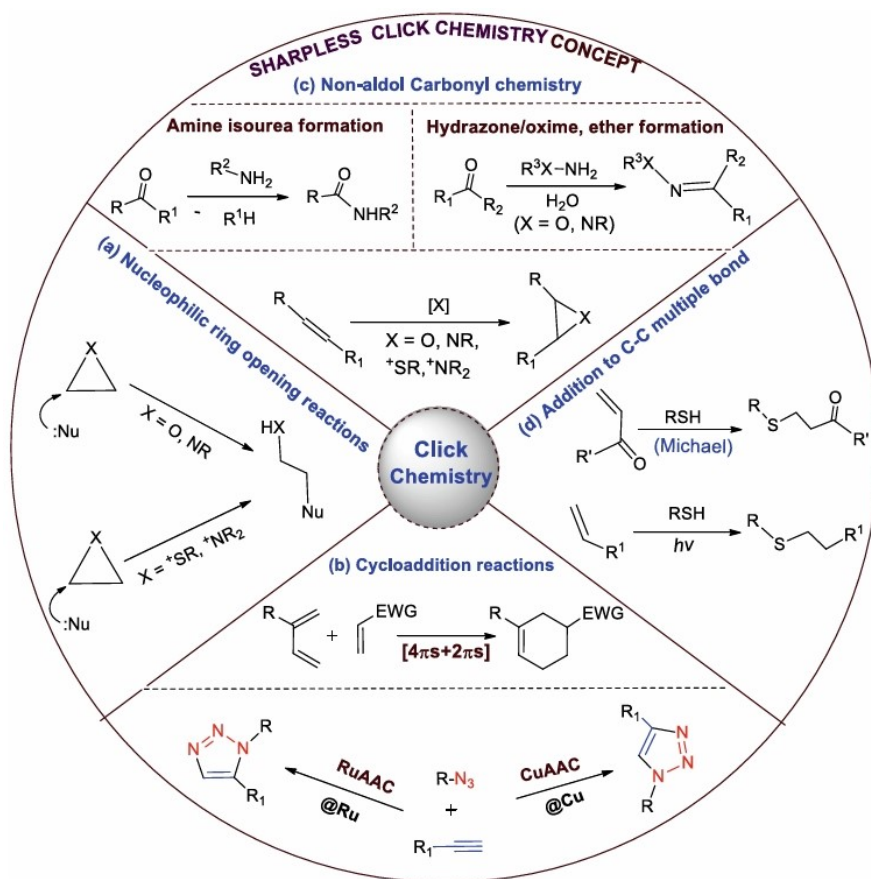
Figure 1.13: Types of Click chemistry

Sharpless classified these reaction in four main categories (**figure 1.13**):

1. Nucleophilic ring opening reactions

2. Cycloaddition reactions

3. Non-aldol Carbonyl chemistry

4. Addition to C-C multiple bond

Then, in the early 2000s, Carolyn R. Bertozzi established the bioorthogonal concept, a set of reactions that[28] :

- Occur at biological pH and temperature

- Occur in a selective and rapid way

- Form a stable and easy to incorporate product

Bioorthogonal reactions involve the incorporation of small functionalities, such as azides, that have excellent accessibility as metabolic precursors.

Bertozzi specifically applied Professor Georg Wigg's Strain-Promoted Azide-Alkyne Cycloaddition (SPAAC) within a biological system. This reaction occurs between strained cyclooctyne and phenyl azide, efficiently producing the corresponding triazole without requiring a catalyst. Known as a copper-free cycloaddition, the lack of a metal catalyst makes this method more suitable for in vivo applications.
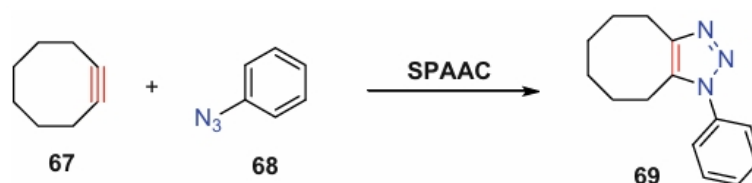
Figure 1.14: Strain-promoted cycloaddition 'copper-free click chemistry' Wittig reaction

1.6 Objectives
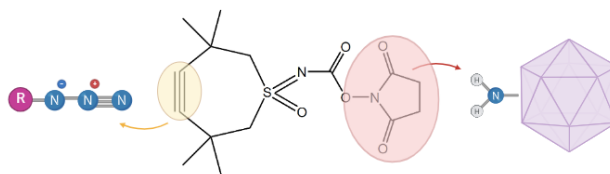
Figure 1.15: Click reaction

The aim of the project, is develope and characterize a technique to covalently coat AAVs with zwitterionic polymers and pBAEs through the Click chemistry. To do that, the main steps are:

- Characterization of CliCr®-Osu as a Functional Linker

- Development of a Click Chemistry Coating Strategy: Characterize the reaction between CliCr®-Osu and AAVs, followed by conjugation with a zwitterionic polymer. Optimize coating parameters, including polymer concentration and reaction conditions.

- Comparison of Coating Strategies to evaluate three distinct approaches:
  - Electrostatic interactions
  - Covalent modifications
  - Click chemistry-enabled linking with zwitterionic polymers

- Asses Cytocompatibility

- Functional Analysis of Coated AAVs

- Synthesis and Characterization of a Modified pBAE Polymer
  - Develop a pBAE polymer modified with an azide group to interact with the CliCr®-Osu group.
  - Thermally characterize the polymer
  - Test the stability of the resulting coated AAVs over time.

- Investigate the ability of zwitterionic polymer coatings to target muscle cells using peptide conjugation.

By achieving these objectives, this work seeks to advance the use of AAVs in gene therapy, particularly for patients with DMD, and to demonstrate the potential of click chemistry as a tool for overcoming key challenges in viral vector development.

Chapter 2

Materials and methods

Hepes and DMSO were purchased from Sigma-Aldrich®.

2.1 Cells

Two different cell lines have been used for this project, maintaining the same conditions of culture: HeLa (ATCC® TIB-71) was used as a permissive and persistent cell line; and C2C12 (ATCC® CRL-1772TM) was used as target cell line. Cells were cultured at 37ºC, under 5% CO2/95% air atmosphere.

PBS and horse serum were purchased from Sigma-Aldrich®. Fetal bovine serum (FBS), Dulbecco's Modified Eagle's Medium (DMEM), Trypsine-EDTA, glutamine, penicillin and streptomycin were purchased from Gibco®.

2.1.1 Maintenance of cells

All the experiments based on this project were preceded by cell media preparation. Cells were thawed from the storage conditions (10E6 cell/mL in FBS 10% DMSO, -80ºC) and transferred into a Petri plate with supplemented DMEM media. DMEM is enriched with 10% (v/v) heat inactivated fetal bovine serum (FBS), 1% (v/v) P/S 100X and 1% (v/v) L-Glutamine 1X. Cells were seeded once they reached approximately 80-90% confluence, making them ready for trypsinization and passaging into a new plate, where they were incubated at 37ºC or used to start transductions.

To freeze them again, a freezing solution with a cryoprotectant was prepared. At first, a solution of 10% DMSO in FS was prepared. Once the cells reached the right confluence, they were trypsinized and counted. Then, they were centrifuged, resuspended in the freezing media to obtain a final density of 10E6 cell/mL, and finally aliquoted at 1 mL per cryovial. The cryovials were then placed in an

isopropanol freezing container (e.g., Mr. Frosty) to cool cells at a rate of -1°C/min and stored in a -80°C freezer for at least 24 hours. Afterward, they were moved to the -150°C freezer for long-term preservation.

2.1.2 Differentiation of C2C12

Differentiation studies were carried out in 96-well plates. First of all, 80 uL of bovine type I collagen (100 ug/ml) per well were added to the wells to pre-treat them and create a better microenviroment for the differentiation. The plate was stored overnight at 4°C. After 24 hours the collagen was aspired and cells were seeded at a concentration of 12E3 cells/well in DMEM 10% FBS medium and incubated at 37ºC in 5% CO2 atmosphere. After 24 hours the medium was aspired, and 150 uL of differentiating medium were added to each well. The differentiation medium consisted of DMEM with 2% (v/v) Horse serum, 1% (v/v) P/S 100X and 1% (v/v) L-Glutamine 1X. 5 days after the seeding, the cells were ready to work. A visual evaluation of the differentiation was performed using the fluorescence microscope Zeiss Axio Vert.A1.

In the **Figure 2.1** we can see how should be the cells during the differentiation.
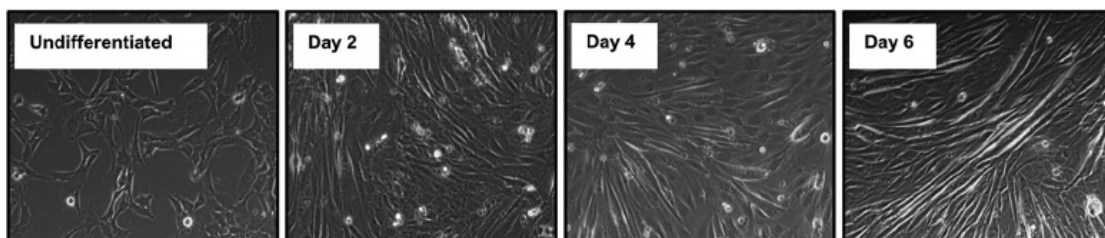
Figure 2.1: C2C12 myoblast differentiation for up to 6 days [29]

2.2 Polymers

2.2.1 Zwitterionic polymers

The zwitterionic polymers used for the preliminar studies, zw1 and zw2, were synthesized by PhD student Antoni Torres Coll using RAFT polymerization. These polymers feature a main chain with branching groups that contain both positive and negative charges, resulting in an overall neutral charge (figure 2.3. Specifically, zw1 and zw2 belong to the family of sulfobetaine-based zwitterionic polymers, which incorporate sulfonate anions and quaternary ammonium cations.

The key difference between zw1 and zw2 lies in their length, which was determined during the polymerization process, with zw1 being shorter than zw2.
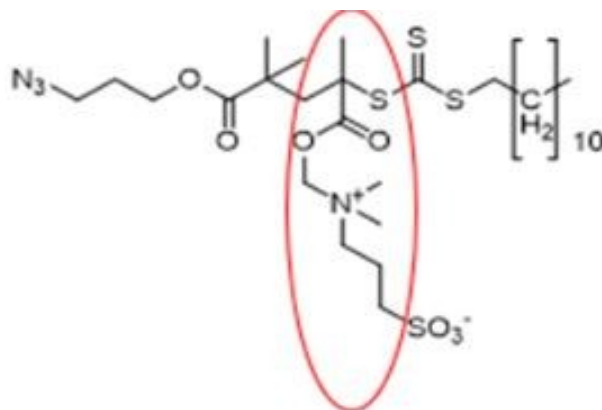
Figure 2.2: Chemical structure of the zwitterionic polymers. In the red circle there is the monomer repetition, that can be formed from 10 to 50 monomers. In this case, the zw1 has 10 repetition (MW 14371 g/mol) and the zw2 has 20 repetitions (MW 28742 g/mol)

The other polymer used was a peptide-functionalized zwitterionic polymer, previously synthesized by the GEMAT group. The peptide 2, which contains a cysteine group (-SH thiol group at the end), is able to form a covalent bond with the acrylate groups at the end of the polymer. The length of the final polymer pep2-zw was similar to the length of the zw2, so was possible to compare them.

2.2.2 Synthesis of the polymer

Synthesis of the C6-pBAE with the N3 group

The synthesis of a C6-pBAE generally consists of a conjugation of primary amines, such as 5-amino-pentanol and 1-hexylamine in a 1:1 molar ratio, with a 1,4-butanediol diacrylates at 1:1.2 molar ratio of amine: diacrylates.
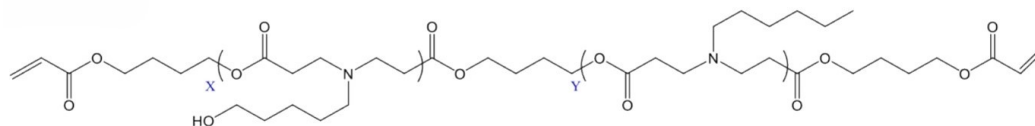
Figure 2.3: Chemical structure of the C6 pBAE backbone

In this case, the desired structure is a C6-pBAE with an azide group. To achieve this, 5-amino-pentanol, 1-hexylamine, and 3-azido-1-pentanol were mixed in a 1:1:1 molar ratio. This mixture was then added to 1,4-butanediol diacrylate in a 1:1 molar ratio. Therefore, the number of moles of 1,4-butanediol diacrylate was the same as the sum of the moles of the other components. Then, the solution was stirred in an oil bath at 40°C for almost 6 hours and then cooled down at room temperature. Tipically, solvent-free synthesis reactions require high temperatures and short reaction times. However, in this case, a lower temperature was employed because 3-azido-1-pentanol begins to degrade at temperatures above 60 °C.

To evaluate the efficiency of the synthesis, a simple mathematical formula is applied:

$$\frac{\text{Final product weight (g)}}{\sum \text{ of the weight of all reagent(g)}} \tag{2.1}$$

Synthesized structures were confirmed by H-NMR and FT-IR analysis.

NMR spectra were recorded in a 400MHz Varian (Varian NMR Instruments, Claredon Hills, IL) and dimethyl sulfoxide-d6 was used as solvent. All data were processed and analyzed using the MestreNova 14.2.0 software.

IR spectrum are obtained using the FT-IR equipment (Thermo SCIENTIFIC model NICOLET IZ10 / DTGS detector in ATR mode).

Adding of the peptide

The pBAE modifications with targeting peptides were achieved through an end-capping reaction of the acrylate-terminated polymer, using a molar ratio of 1:2.4 (C6-pBAE: peptide) in dimethyl sulfoxide (DMSO). The reaction mixture was stirred overnight at room temperature. The modified polymer was then isolated through precipitation in a diethyl ether and acetone mixture at a 7:3 (v/v) ratio and then dried under vacuum.

2.2.3   Characterization of the polymer C6N3 pBAE

To perform a comprehensive thermal characterization, the polymer was analyzed using Differential Scanning Calorimetry (DSC) and Thermogravimetric Analysis (TGA).

DSC

The first analysis was conducted from -35 °C to 300 °C under a nitrogen atmosphere, with a heating rate of 10°C/min. In contrast, the second analysis was carried out from -35 °C to 190 °C. Both analyses were performed using the DSC 214 Polyma instrument by Netzsch.

TGA

The first analysis was carried out from room temperature to 900 °C in an air atmosphere. The second analysis was performed from room temperature to 500 °C in an inert atmosphere, followed by cooling to 300 °C, and then reheating to 900 °C in air. Both analyses were performed using the Thermal Analysis System TGA 2 by Mettler Toledo.

2.3   Polymeric coating

AAV vectors were produced by the Viral Vector Production Unit (UPV) of the Universitat Autònoma de Barcelona. AAV9-GFP (Physical titer: 1,26E+13 vp/mL) and AAV9-Luc (Physical titer: 9,34E+12 vp/mL) were purified by PEG precipitation / Iodixanol gradient and were stored in PBS-MK / 40% Iodixanol.

Zwitterionic and C6-N3 pBAE with Click Chemistry
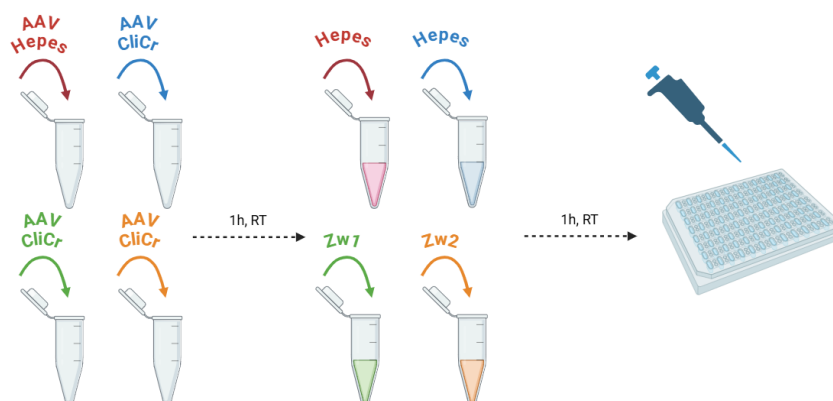
Figure 2.4: Scheme of the procedure of coating

1E9 viral particles (VPs) of AAV solution was thoroughly mixed with the CliCr®-Osu molecule in HEPES buffer (20 mM, pH 8). The buffer volume was adjusted to achieve a total volume of 20 µL. This mixture was incubated at room temperature (R.T.) for 1 hour before adding the polymer solution. Different coating percentages of CliCr®-Osu molecule were tested. To determine the required quantity for each percentage, the total number of free amines was calculated based on the total viral particles (VPs) and the number of free amines per viral particle (480 free amines/VP). Using the total number of free amines and the molar mass of the

CliCr®-Osu molecule, the volume needed to achieve the desired coating percentages was determined.

Simultaneously, during the first hour of incubation, the required amounts of polymers (Zw1, Zw2 or C6N3) for different coating percentages were prepared. The required quantities were determined by adjusting the molar ratios between the CliCr®-Osu molecule and the polymers.

Finally, the polymer solution was added to the AAV solution, thoroughly mixed by pipetting, and incubated for another hour at R.T.

Zwitterionic and C6-NHS pBAE

Two separate solutions were prepared: (a) Hepes (20 mM at pH 7.4) - polymer, and (b) Hepes (20 mM at pH 7.4) - AAV. Polymer mixture (a) is then added to mixture (b) by slowly pipetting (30 times), followed by an incubation of 30 minutes at room temperature (RT). Uncoated particles follow the same coating protocol only by adding the buffer in solution (a).

2.3.1 Zeta potential analysis

The surface charge, also referred to as the zeta potential (Z-potential), of both coated and uncoated viral vector preparations was measured using the Dynamic Light Scattering (DLS) technique (ZetaSizer Nano SZ, Malvern Instruments Ltd, United Kingdom, 4-mW, 633 nm laser). To prepare the samples for analysis, a concentration of 5E10 viral particles (VP) was used. Each sample was further diluted in milliQ water at a 1:10 ratio to ensure optimal conditions for measurement. For each sample, three measurements were conducted, with 20 runs per measurement, using intensity-based analysis. The results are reported as the mean ± standard deviation from at least three independent batches.

2.3.2 Cytotoxicity protocol (MTT assay)

To verify the safety of the high concentration of CliCr®-Osu reagent and polymers, citotoxicity studies were conducted in 96-well plates.

The samples were analyzed 72 hours after the transduction. To do this, the medium in the plate was removed and 100 ul of a MTT solution was added to each well, at a final concentration of 0,5 mg/ml MTT on DMEM 10% FBS. The plate was then incubated at 37°C for 1 hour. After incubation, the MTT solution was replaced with 100 μL of DMSO per well to dissolve the crystals formed during the process. To dissolve the crystals more efficiently, can be useful shaking the plate. Finally, the plate was placed in the Infinite Mplex (TECAN®) reader, and the absorbance of the samples was measured at a wavelength of 570 nm. The resulting
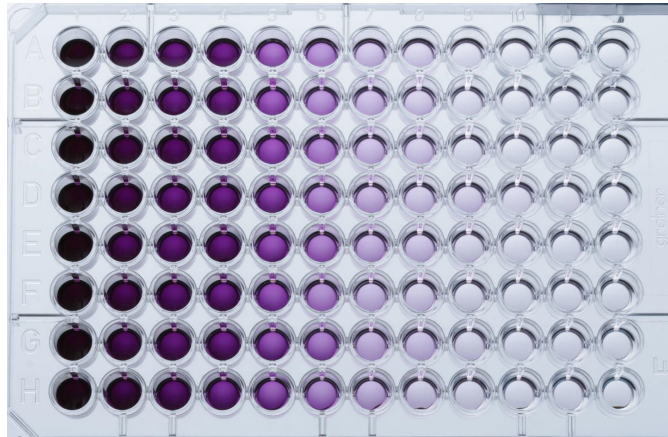
Figure 2.5: Example of MTT assay results

data were interpreted using the following formula:

$$\text{Survival rate (\%)} = \frac{A_{\text{sample}} - A_{\text{blank}}}{A_{\text{control}} - A_{\text{blank}}} \times 100 \tag{2.2}$$

MTT reagent was purchased form ThermoFisher.

2.3.3 Labeling AAV particles

AAVs were incubated with the CliCr®-Osu group for 1 hour. The binding reaction was carried out from the volume corresponding to 10E10 vp and various percentages of the CliCr®-Osu group, reaching a final volume of 20 µL by adding hepes buffer (20 mM pH 8,5). Following this, the samples were incubated with the fluorophores Cy5-NHS and Cy3-N3 for an additional hour at room temperature under dark conditions.

(a) Chemical structure of the Cy5-NHS

(b) Chemical structure of the Cy3-N3
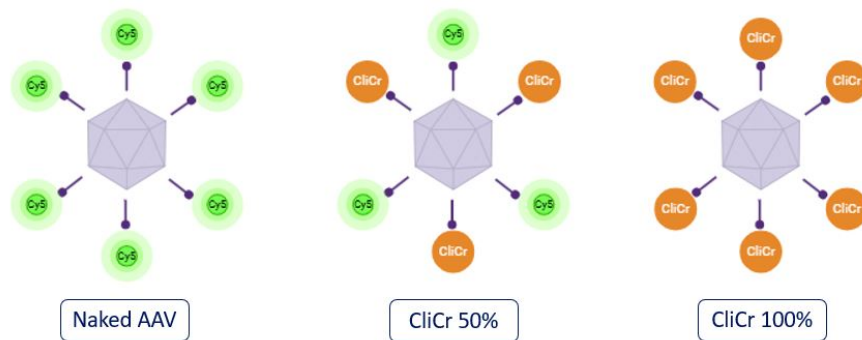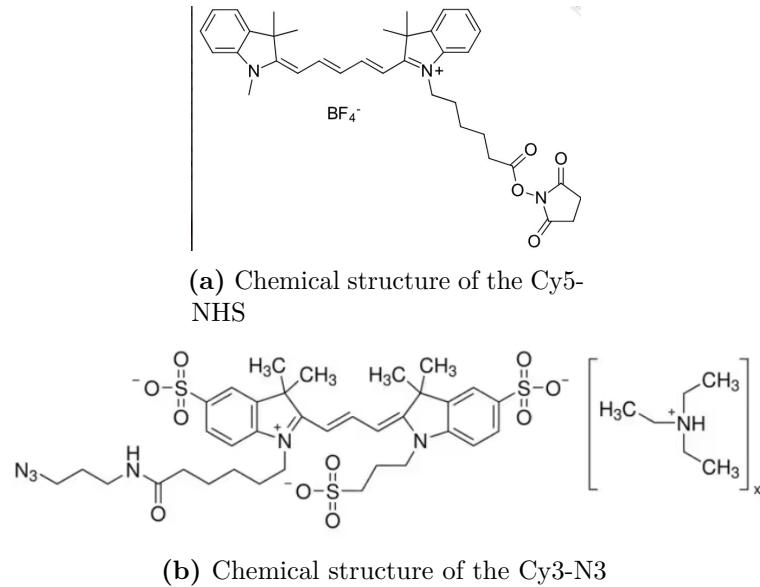
Figure 2.7: Fluorescence analysis with the Cy5

The NHS ester group of the Cy5-NHS reacts with primary amines (-NH2) on AAV, forming a stable amide bond.

28
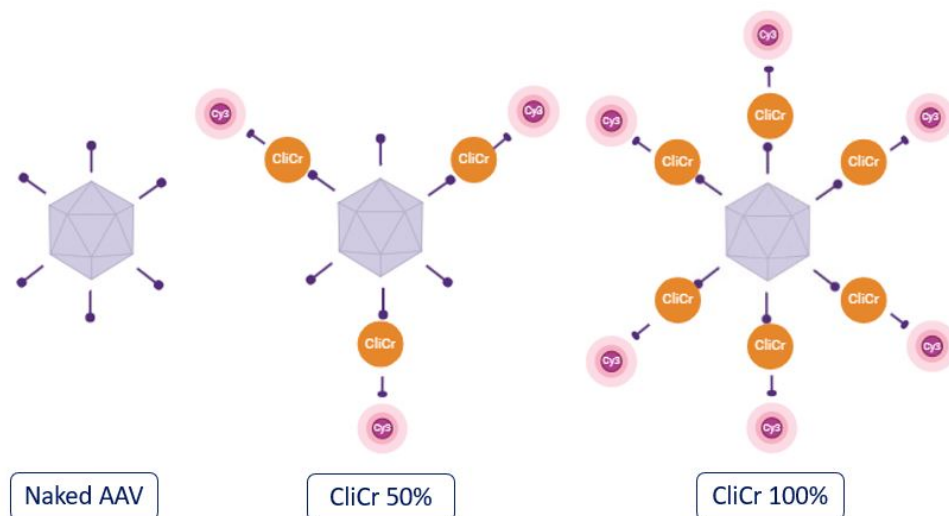
Figure 2.8: Fluorescence analysis with the Cy3

The azide group (-N3) of Cy3-N3 can instead undergo a strain-promoted azide-alkyne cycloaddition (SPAAC) with a molecule that contains an alkyne group, resulting in the formation of a covalent bond.

Once labeled, AAV particles were separated from unconjugated dye by ultra-filtration through AMICON® devices, using 20 mM HEPES buffer at pH 8.5 for washing. After each centrifugation cycle, the supernatant was collected and transferred into an Eppendorf tube. The Amicon tube was then inverted and subjected to a final centrifugation to collect the labeled AAV particles. Subsequently, all samples were analyzed using a plate reader to measure the fluorescence intensity. The fluorescence of the samples was measured at wavelengths of excitation of 630 nm and emission of 667 nm. For the Cy5-NHS, instead, the wavelengths were 550 nm and 570 nm.

Cyanine5-NHS ester fluorophore was from Lumiprobe for immunochemistry assays and polymer labeling, while Cyanine3-N3 was purchased from Merck. AMI-CON centrifugal filters Ultra 0.5 mL (50k) devices were purchased from Merck.

2.3.4 Transduction studies

Transduction studies were carried out in 96-well plates. Cells were seeded at a concentration of 8E3 cells/well in DMEM 10% FBS medium and incubated at 37ºC in 5% CO2 atmosphere 24h before the vectors were added. After the incubation time, the media was removed, and the cells were washed with 1X PBS to eliminate any cells that had not adhered to the surface of the plate. Then, 50 µL of the virus particle solution (either naked or coated) in DMEM with 2% FBS was added to each well. The AAV multiplicity of infection (MOI) used was 1E5 vp/cell, resulting in the addition of 8E8 vp per well. For each condition analyzed, triplicates were prepared, together with negative controls (untreated cells and DMEM with 2% FBS).

After the initial 24 hours post-transduction, 150 µL of DMEM with 10% FBS were added per well to prevent desiccation. Following 72h of incubation, the cells were washed with PBS, trypsinized, and then fixed with 2% PFA in 1X PBS. For each well, 25 µL of trypsin-EDTA, 50 µL of DMEM with 10% FBS, and 25 µL of PFA were added. The AAV9-GFP expression was quantified by flow cytometry (NovoCyte, ACEA Biosciences) and compared with the negative controls.

Chapter 3

Results and Discussion

3.1 Synthesis and characterization of Polymers

For the purpose of this thesis, two different polymers were utilized to achieve polymer-coated AAVs through Click Chemistry, both incorporating specific peptides to confer targeted delivery properties. Both approaches will be described in detail. However, greater emphasis will be placed on pBAE, as we personally synthesized it and performed a more in-depth analysis within the framework of my research.

Infact, to introduce an additional control in the click chemistry strategy and assess its effectiveness, we synthesized a modified C6 pBAE polymer incorporating an azide group on its lateral chain and targeting moieties on both terminal sides of the polymeric structure (**figure 3.1**).

This functionalization enables specific binding to the CliCr group via azide-alkyne cycloaddition, facilitating a more stable and targeted conjugation process while minimizing non-specific interactions.
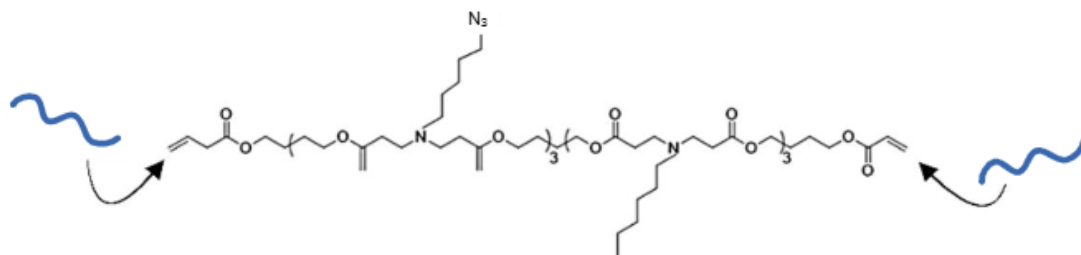
Figure 3.1: Schematic representation of a pBAE chain with terminal ends acrylate groups for the grafting of peptides (in blue) via cysteine thiol groups, and the azido group on the lateral chain

3.1.1   C6-OM-pBAE-N3

Before starting the polymer synthesis, we first analyzed one of the key components, 3-azido-1-propanamine, to ensure it would remain stable under the chosen reaction conditions. This step was important because previous reports indicated that 3-azido-1-propanamine begins to degrade at temperatures above 60°C. To avoid this issue, we lowered the synthesis temperature to 40°C and confirmed through IR analysis that the compound remained stable at this temperature.

Once the polymer was synthesized, we performed IR spectroscopy to confirm the successful incorporation of the azide group into the C6 pBAE polymer. A distinct peak at 2069 cm-1, corresponding to the azide (–N3) stretching vibration, was clearly visible in the spectrum(**figure 3.3**). This confirmed the presence of the azide group in the polymer structure.

The spectrum also showed additional peaks characteristic of the polymer backbone. A strong absorption at 1730 cm^{-1} confirmed the presence of ester (C=O) groups, while the aliphatic C–H stretching vibrations appeared between 2800–3000 cm^{-1}, as expected. The broader peaks in the ∼1200–1600 cm^{-1} range represent various C–C and C–O stretching and bending vibrations characteristic of the pBAE structure. No unexpected peaks were detected, suggesting that the synthesis process was clean and did not introduce significant impurities or by-products. These results confirmed that the polymerization was successful under the adjusted conditions, preserving the azide group while maintaining the structural integrity of the C6 pBAE backbone.
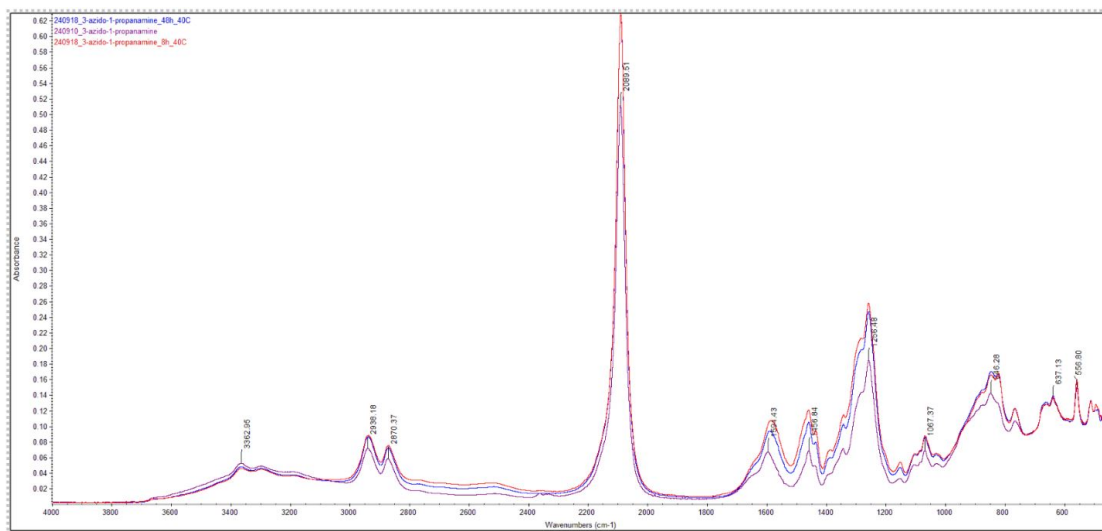
Figure 3.2: IR spectra of 3-azido-1-propanamine under different conditions. The purple spectrum represents the component before heating, the red spectrum shows the component after 8 hours at 40°C, and the blue spectrum illustrates its state after 48 hours at 40°C.
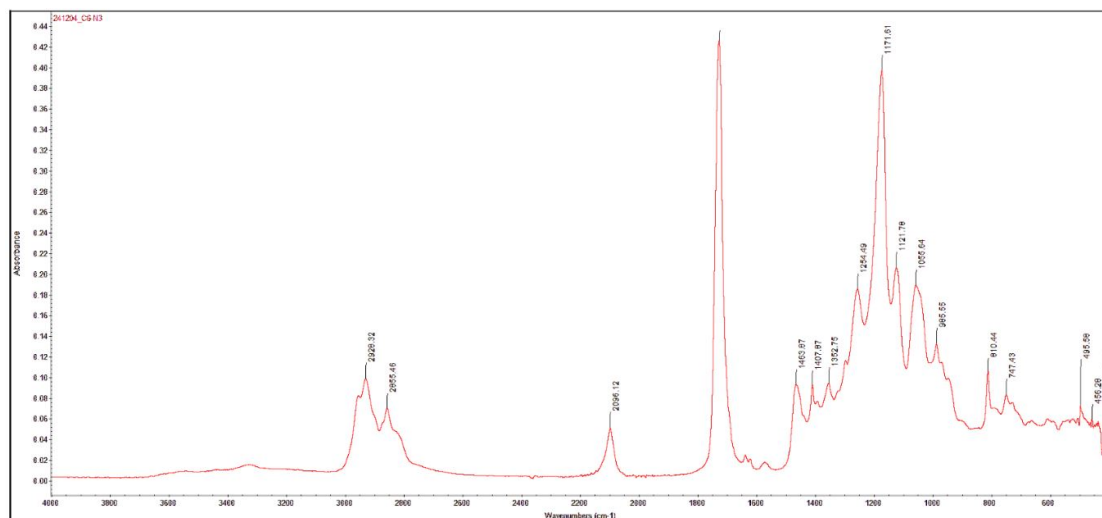
Figure 3.3: IR spectrum of the polymer synthetized

The chemical structure and functionalization of the synthesized polymers were confirmed using Nuclear Magnetic Resonance (NMR) spectroscopy. The NMR spectra of C6 pBAE and C6 pBAE functionalized with an azide (N3) group are presented in **Figure 3.4** and **Figure 3.5**.

C6 pBAE Spectrum

The spectrum of C6 pBAE (**figure 3.4**) shows characteristic peaks corresponding to the protons of the pBAE backbone. Signals in the region of **δ 0.8–2.2 ppm** are attributed to the aliphatic protons from the methylene and methyl groups in the polymer chain. The peaks in the **δ 3.4–4.2 ppm** region are associated with protons adjacent to the ester and secondary amine groups, which are key features of the pBAE structure. The absence of unexpected peaks in the spectrum confirms the successful synthesis of the polymer without significant impurities.

C6 pBAE Functionalized with Azide Group

The spectrum of C6 pBAE with an azide group (**figure 3.5**) retains the characteristic peaks of the pBAE backbone, confirming that the structural integrity of the polymer was maintained during the azide functionalization process. In addition, new signals were observed in the **δ 3.0–3.5 ppm** region, which correspond to the methylene protons adjacent to the azide group. The presence of these peaks confirms the successful incorporation of the 3-azido-1-propanamine moiety into the polymer chain. The signal in this NMR spectrum is weaker than that of C6 pBAE, possibly due to a lower concentration of the polymer dissolved in DMSO.

Comparison of the Spectra

While the backbone signals are consistent, the appearance of the new peaks specific to the azide group in the functionalized polymer provides clear evidence of successful modification. Additionally, the absence of broadening or significant shifts in the backbone signals suggests that the reaction conditions used for functionalization did not lead to polymer degradation.

These results demonstrate the successful synthesis of C6 pBAE functionalized with an azide group. The azide functionality adds versatility to the polymer, enabling its potential use in click chemistry reactions. Furthermore, the integrity of the polymer backbone after functionalization highlights the robustness of the synthesis and modification protocols.
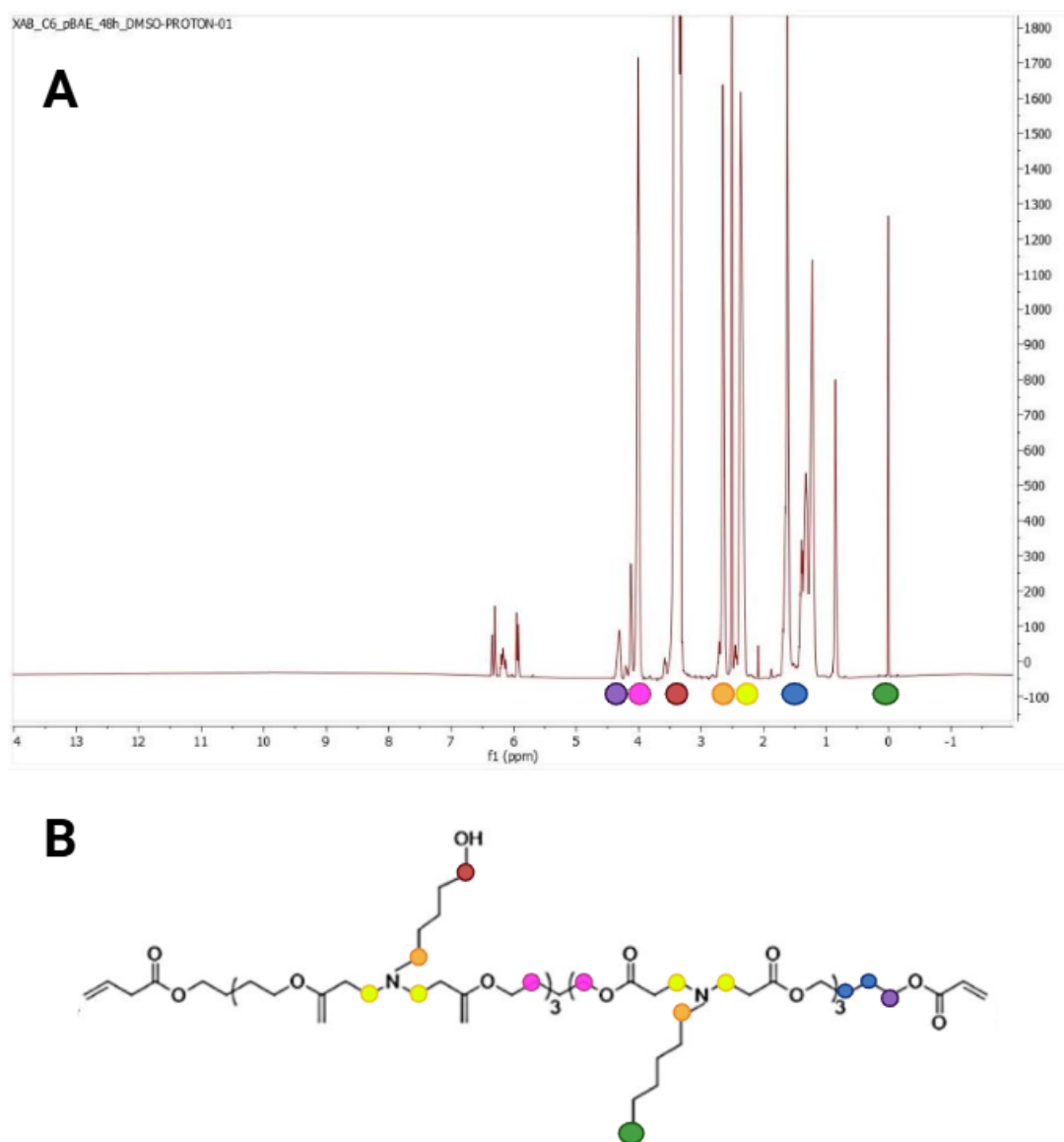
Figure 3.4: A) 'H-NMR spectra of C6 pBAE dissolved in DMSO; B) molecular structure of C6 pBAE polymer chain
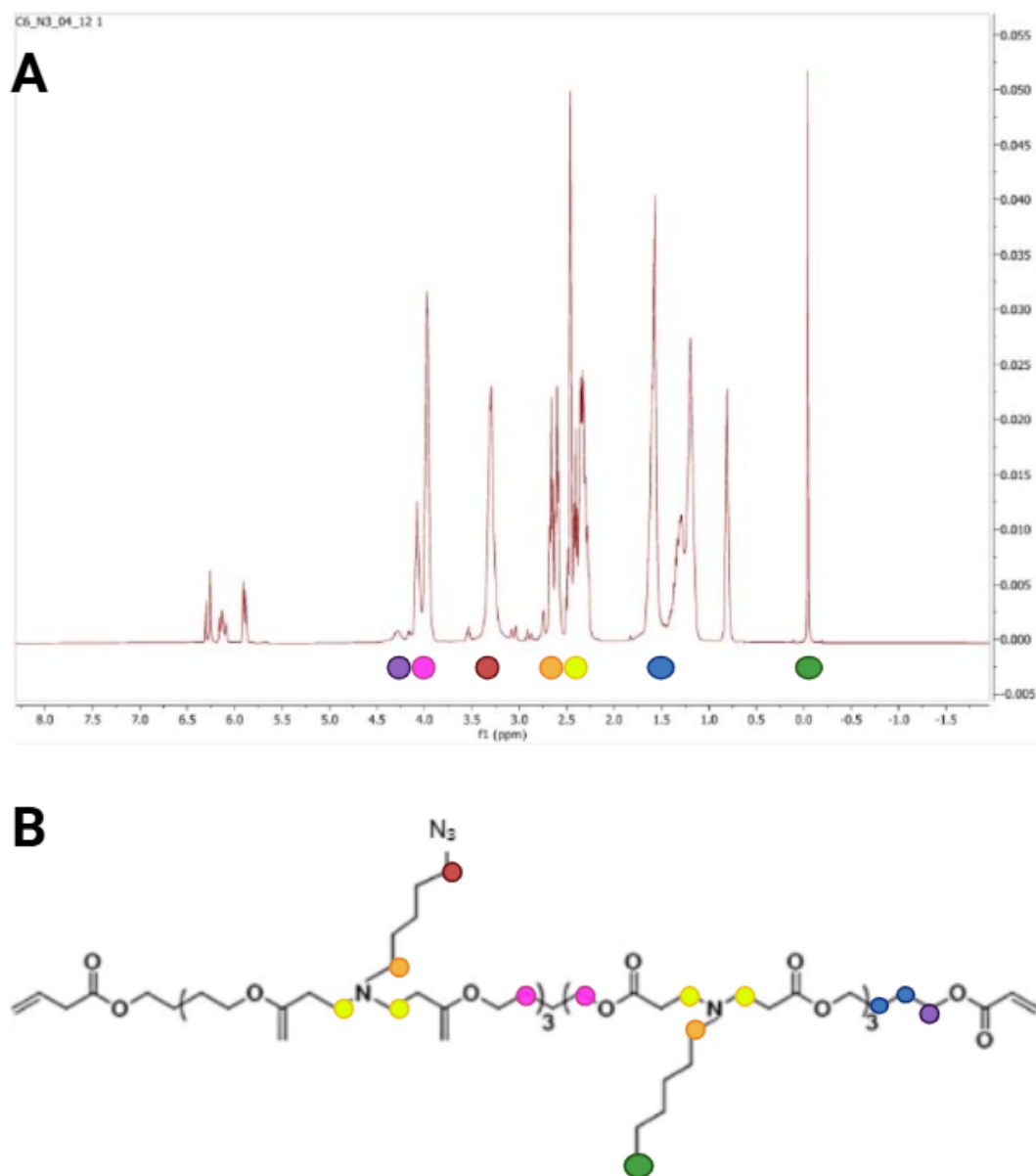
Figure 3.5: A) 'H-NMR spectra of C6-N3 pBAE dissolved in DMSO; B) molecular structure of C6-N3 pBAE polymer chain

To continue with the characterization of the polymer, Differential Scanning Calorimetry (DSC) was performed to analyze the thermal properties of the synthesized polymer, C6 pBAE functionalized with an azide (N3) group.

DSC is a thermo-analytical technique that measures physical and chemical changes in a material as a function of temperature or time. It provides crucial information about endothermic processes (e.g., melting, glass transition) and exothermic processes (e.g., crystallization, decomposition). For polymers, the thermal behavior detected by DSC depends on several factors, including the polymer type, molecular weight, degree of crystallinity, crosslinking, and the presence of additives or fillers. This technique is particularly useful for determining critical properties such as the glass transition temperature (Tg), melting temperature (Tm), and thermal stability.

Two sets of experiments were conducted. The DSC thermograms display key thermal events, including melting transitions, crystallization peaks, and decomposition stages. Below, the observed transitions and their associated thermal parameters are discussed in detail.

First Set of Measurements:

Sample 1 has been analysed from -35°C to 300°C with the following temperature program: cooling from 25 °C to -35 °C at a rate of 10 °C/min, followed by an isothermal hold at -35 °C for 5 minutes, and concluded with heating from -35 °C to 300 °C at a rate of 10 °C/min. The analysis was performed twice using two different samples to ensure repeatability, given the unusual profile observed in the decomposition peak around 270 °C (**figure 3.6**).

- **First Complex Peak**
  Peak temperature: 61.1 °C
  Enthalpy change (ΔH): -5.42 J/g
  This minor endothermic peak suggests a transition that may correspond to the relaxation or partial melting of low-crystallinity regions.

- **Second Complex Peak**:
  Peak temperature: 185.7 °C
  Enthalpy change (ΔH): 89.56 J/g
  This significant endothermic peak is indicative of a melting transition, likely associated with crystalline domains in the polymer matrix.

- **Decomposition Transition**:
  Peak temperature: 267.3 °C
  Enthalpy change (ΔH): -248.2 J/g
  This highly exothermic event corresponds to the thermal degradation of the polymer.

Second Set of Measurements:

This second measurement was conducted under the same conditions but with a narrower temperature range to better characterize the nature of the peak appearing around 185°C. Sample 2 was analyzed with a temperature program that began with a ramp from 25°C to -35°C at 10°C/min. The temperature was then maintained at -35°C for 5 minutes before being increased to 190°C at the same rate of 10°C/min. Once 190°C was reached, the temperature was lowered back to -35°C at 10°C/min, followed by a second heating cycle using the same temperature program (**figure 3.7**).

- **Initial Transition**
  Peak temperature: 69.4 °C
  Enthalpy change (ΔH): -4.43 J/g
  This minor peak reflects similar behavior as the first complex peak in the first measurement, suggesting comparable low-energy transitions.

- **Major Melting Transition**:
  Peak temperature: 185.2 °C
  This peak confirms the crystalline melting observed in the first set of data, providing reproducibility and consistency between measurements. In the second heating step, this peak disappeared.

The results confirm the semi-crystalline nature of the synthesized polymer. The melting transition at approximately 185 °C is consistent across measurements, indicating the presence of ordered crystalline regions within the polymer structure. Additionally, the degradation event at higher temperatures (>260 °C) demonstrates that the polymer exhibits good thermal stability.

The initial minor peaks (61.1 °C and 69.4 °C) could be attributed to localized transitions such as glass transition phenomena or melting of small crystalline regions formed during synthesis. Alternatively, this peak might correspond to the evaporation of residual solvent employed during the synthesis process.

The thermal stability and well-defined melting transitions make the C6 pBAE with N3 group a promising candidate for applications requiring controlled thermal behavior, such as in biomedical devices or advanced polymer composites.

Further analysis, such as thermogravimetric analysis (TGA), could complement the DSC results to provide a comprehensive understanding of the polymer's thermal degradation pathway and enhance its potential application scope.
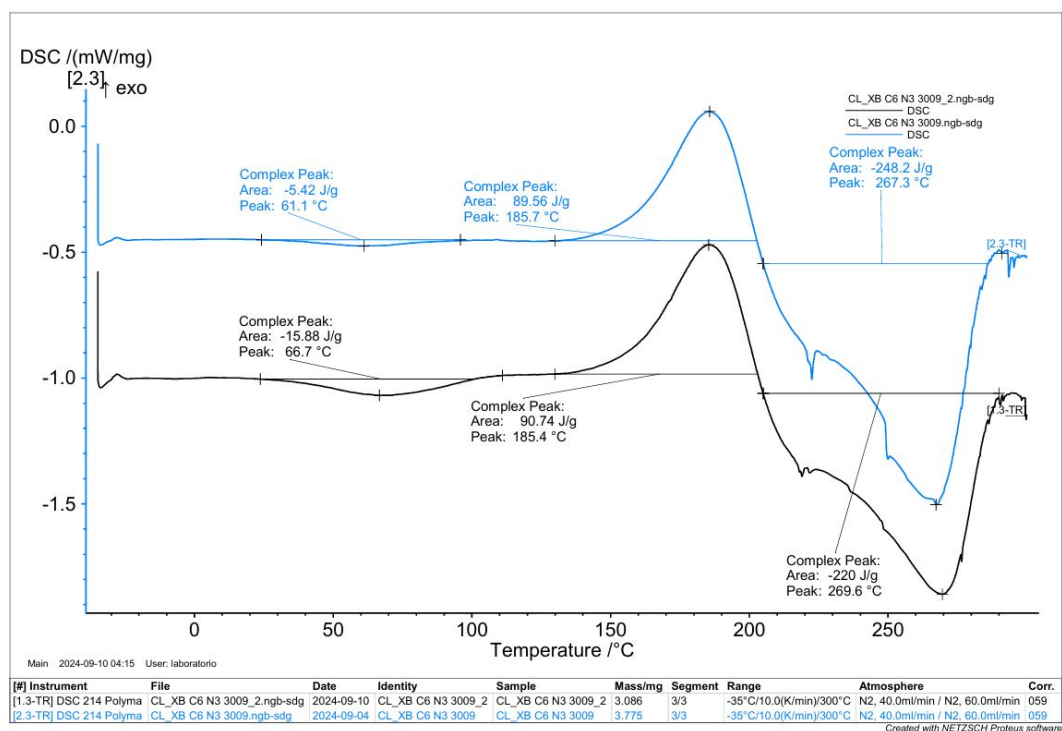
Figure 3.6: DSC sample 1 [-35°C;300°C]
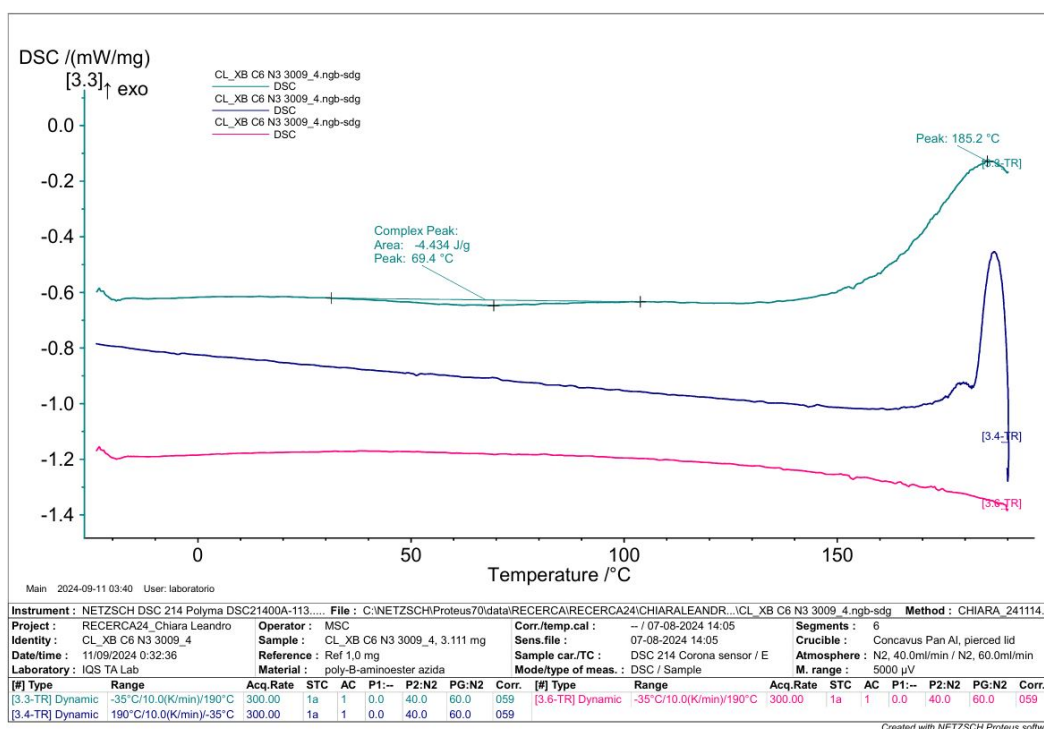
Figure 3.7: DSC sample 2 [-35°C; 190°C]
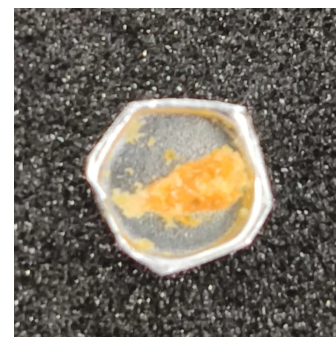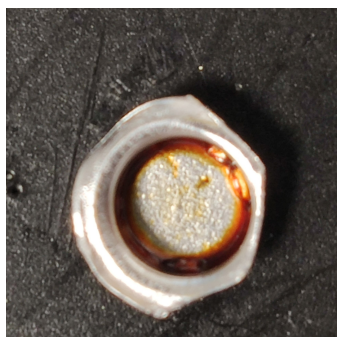
Figure 3.8: Samples after the heating process: (a) Sample heated up to 300°C: we can see that the sample is melted and highly decomposed; (b) Sample heated up to 190°C: we can see a change in the color, that became yellowish due to any kind of decomposition, not as aggressive like the one observed at 300°C

40

To analyze the behavior of two samples under different temperature conditions we have used Thermogravimetric Analysis (TGA). TGA was employed to gain insights into the thermal stability of the samples, as well as to identify any decomposition, oxidation, or other significant changes in mass during the temperature ramps. TGA, monitors the weight changes of a material as it is heated, cooled, or held at a constant temperature.

In the first experiment, the sample was heated from room temperature (RT) to 500°C in an inert atmosphere to prevent oxidation. TGA measurements helped identify mass loss due to volatile components. After cooling to 300°C, the sample was reheated to 900°C in air to observe its response to oxidation. The residue left at the end of the first heating cycle to 500 °C in an inert atmosphere is 95.4553%, indicating that most of the mass loss is due to volatile components. Upon reheating the sample to 900 °C in air, additional mass loss occurs, leaving a final residue of 10.6344% of the original weight. This indicates oxidation and decomposition of the remaining material (**figure 3.9**).
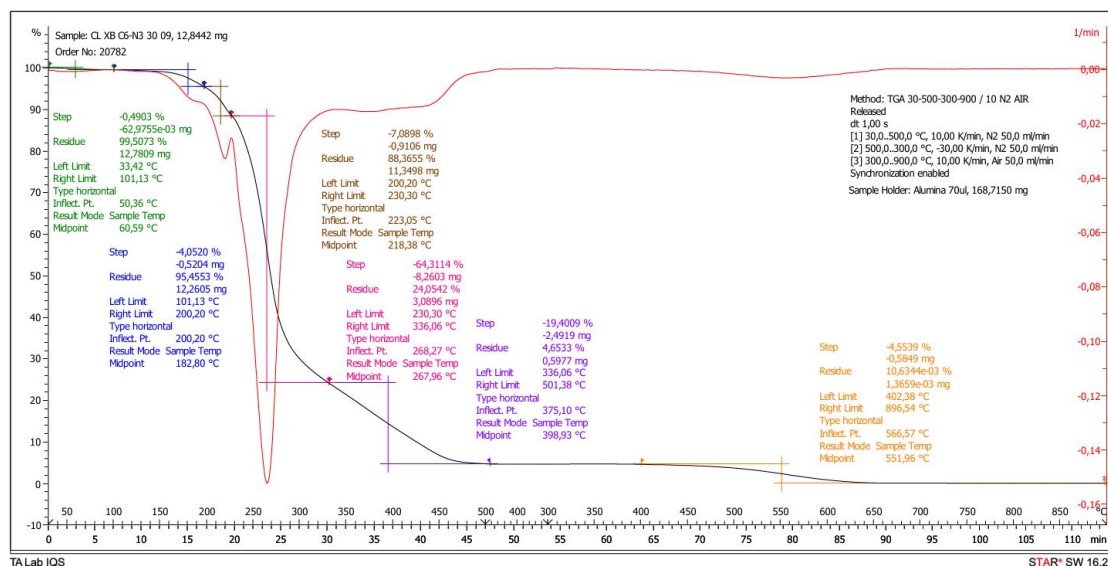
Figure 3.9: First experiment of TGA

41

To determine whether the polymer would degrade or behave differently under varying conditions, it was analyzed a second time exclusively in air.

In this experiment, the polymer was directly heated from room temperature to 900°C in an air atmosphere. The residue left at the end of the analysis is 13.3092%, suggesting slightly higher thermal stability compared to the first experiment. The continuous heating in air leads to overlapping degradation and oxidation processes (**figure 3.10**).
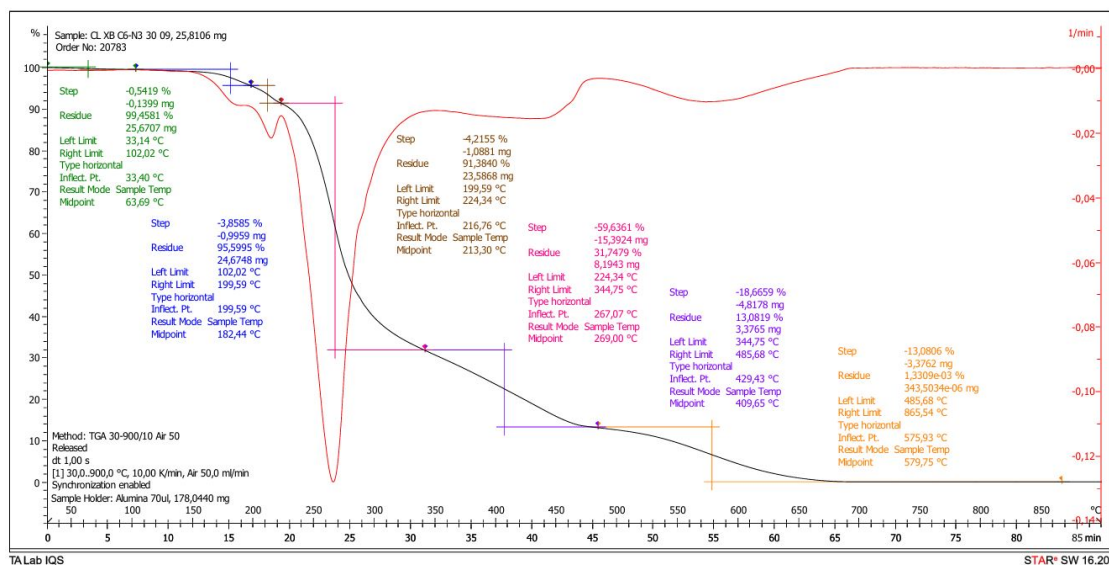
Figure 3.10: Second experiment of TGA

The two TGA curves highlight the impact of experimental conditions on the thermal behavior of the polymer: In the first experiment, the stepwise heating protocol allowed the identification of distinct mass loss events due to volatile components in an inert atmosphere and subsequent oxidation in air. The residue left after oxidation (10.6344%) is lower than in the second experiment. In the second experiment, direct heating in air resulted in simultaneous decomposition and oxidation, leading to a higher final residue (13.3092%).

These results demonstrate how heating conditions, such as the atmosphere and temperature profile, influence the thermal stability, decomposition mechanisms, and oxidation behavior of the C6 pBAE polymer with an N3 group.

42

3.2   Preliminary studies

Once the polymer was successfully synthesized and characterized, the next step was to evaluate the coating process and assess its effectiveness. This involved analyzing the stability of the polymeric coating, its interaction with the AAV surface, and its ability to shield or modify the viral properties. To achieve this, we employed techniques such as zeta potential measurements to monitor surface charge changes and transduction assays to assess functional impact.

3.2.1   Coating characterization

Zeta potential measurements were conducted to assess changes in the surface charge of AAV particles after coating. The expectation was that the zeta potential would become less negative after the coating, particularly with the addition of the zwitterionic polymer, which should theoretically bring the surface charge closer to neutrality.

As seen in **Figure 3.11**, when AAVs were coated with CliCr alone, the zeta potential became less negative, indicating some modification of the surface charge. However, with the addition of the zwitterionic polymer (CliCr+zw1 and CliCr+zw2), the zeta potential became more negative again, which is the opposite of what was expected. The zwitterionic coating was expected to neutralize the surface charge, but the results do not align with this prediction. In the plot, a trend toward increased overall negative charge can be observed when comparing all coated AAV samples to the unmodified virus ("naked"). However, this decrease in charge is not statistically significant.

This unexpected behavior could be due to multiple factors, such as incomplete coating, interactions between the zwitterionic groups and the surrounding medium, or experimental variability. Moreover, the high sensitivity of zeta potential measurements to ionic strength and pH may have contributed to the variability in the data, making interpretation challenging. Further investigations are needed to gain a deeper understanding of the influence of the zwitterionic polymer on the surface charge and to optimize the coating strategy. For this reason, to determine if the coating with the zwitterionic polymers was taking place or not, transduction assays were conducted afterwards.

43
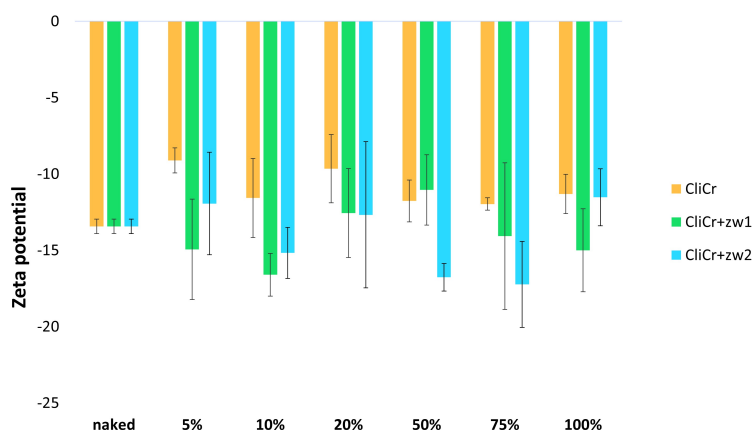
Figure 3.11: Z-potential measurements of the AAV naked and coated with different percentages of the zwitterionic polymer 1 (zw1) and zwitterionic polymer 2 (zw2) bound also with different percentages of CliCr®-Osu (5%, 10%, 20%, 50%, 75% and 100%). The percentages used are the same for the CliCr molecule and the zwitterionic polymers (1:1 molar ratio). The mean of the 3 measurements per sample, done by the DLS, and the Standard Deviation are plotted.

3.2.2 Transduction studies

CliCr concentration up to 100%

To determine the optimal concentrations of the CliCr group and zwitterionic polymers for efficient AAV coating, preliminary studies were conducted using HeLa cells. The HeLa cell line was used in all experiments due to its greater permissiveness compared to C2C12 cells, facilitating easier viral infection. This allowed us to assess the effectiveness of the coating, as we expected a decrease in viral entry with the zwitterionic polymer coating. This reduction occurs because the capsid structure is modified by CliCr and the polymer, which hinders AAV receptor recognition and subsequently limits viral entry into the cells.

Initially, we tested CliCr concentrations ranging from 10% to 100% and zwitterionic polymers with a molecular ratio 1:1 with the CliCr group. These percentages were selected based on prior work conducted by the GEMAT group, who had explored similar ranges but had expressed uncertainty regarding the efficiency of the coating process. Transduction experiments with these concentrations revealed that the coating was not sufficiently effective, likely due to an inadequate amount of CliCr available for the reaction. See **Figure3.12**. In some samples, for both the CliCr alone and CliCr+zw1, a certain cell death was also observed, but the results were still representative enough. To study if the zwitterionic polymers or the CliCr molecule were toxic and therefore, killing the cells, some MTT assays were carried

out simultaneously with the transduction assays. The results obtained are discussed in *Section 3.3*.

Figure 3.12: Level of expression of GFP in HeLa cell line 72 hours after transduction. The assay was performed with the AAV naked (control) and the AAV coated with 5%, 10%, 20%, 50%, 75% and 100% of the zwitterionic polymer 1 (zw1) in green and the zwitterionic polymer 2 (zw2) in blue, previously bound with the same percentages of CliCr®-Osu. The percentages used are the same for the CliCr molecule and the zwitterionic polymer, as they follow a 1:1 molar ratio. The mean of the 3 measurements per sample, done by the Cytometer, and the Standard Deviation are plotted. The conditions used for the experiment were: 8000 cells per well and an MOI of 100,000.

Due to the fact that the amount of reagent seemed too low, the CliCr concentration was progressively increased, with levels tested up to 300%. This approach was guided by findings in the literature, which reported the use of other components for click chemistry reactions in significant excess to enhance reaction efficiency[16].

As shown in the **Figure3.13**, for AAVs coated with CliCr alone, the transduction efficiency increased for all tested percentages compared to the naked AAVs. A possible explanation as to why this happens could be that the CliCr molecule seems to modify the capsid structure of the virus in such a way that facilitates its entrance into the cells. However, with the addition of the zwitterionic polymers (zw1 and zw2), a slight decrease in transduction efficiency was observed comparing with the CliCr alone. Overall, the results indicate that while the coatings had minimal

impact on transduction efficiency, further refinement of the polymer concentration may be necessary to achieve a more significant effect.
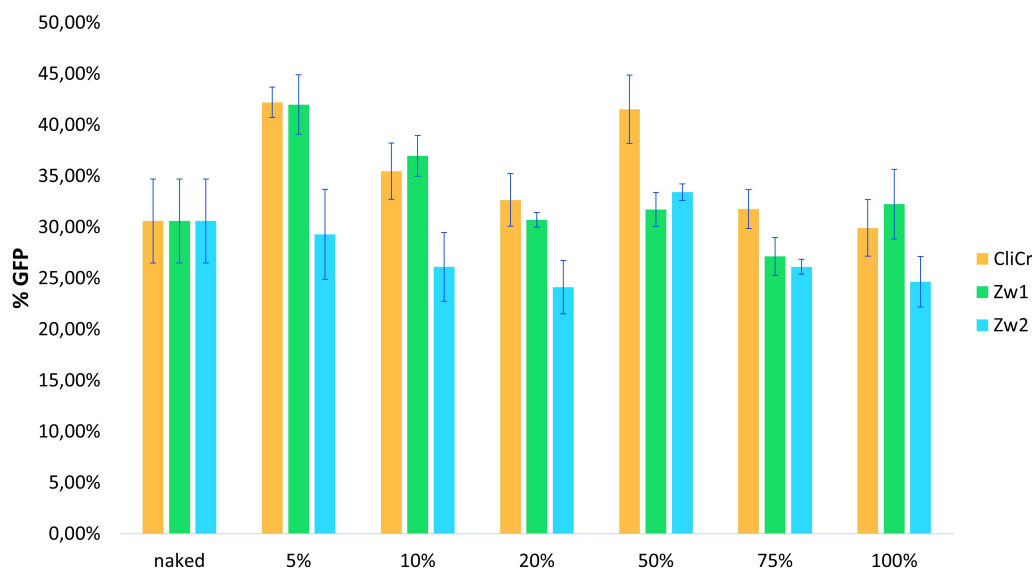

Figure 3.13: Level of expression of GFP in HeLa cell line 72 hours after transduction. The assay was performed with the AAV naked (control) and the AAV coated with 10%, 50%, 100%, 200% and 300% of the zwitterionic polymer 1 (zw1) in green and the zwitterionic polymer 2 (zw2) in blue, previously bound with the same percentages of CliCr®-Osu. The percentages used are the same for the CliCr molecule and the zwitterionic polymer, as they follow a 1:1 molar ratio. "naked+zw1" and "naked+zw2" were added as additional controls. The mean of the 3 measurements per sample, done by the Cytometer, and the Standard Deviation are plotted. The conditions used for the experiments were the same: 8000 cells per well and an MOI of 100,000.

To determine whether the issue was the second reaction between the CliCr group and the polymers, we needed to conduct transduction studies with an excess of polymers. Therefore, we performed transduction experiments using CliCr at 500% and varying the molar ratios of zw1 and zw2.

In the **Figure3.14**, the pink and dark blue bars represent the controls, where AAVs are mixed only with the zwitterionic polymers. Since the zwitterionic polymers cannot bind directly to the AAV surface without CliCr acting as a bridge, these conditions do not result in a true coating and, therefore, maintain transduction efficiency similar to naked AAV. The green and light blue bars, instead, represent AAVs coated with both CliCr and the zwitterionic polymers, allowing for an evaluation of the impact of this dual modification.

The results show that transduction efficiency remains nearly constant for AAVs mixed only with zwitterionic polymers, confirming that, in the absence of CliCr, these polymers do not adhere to the viral surface. However, when CliCr is introduced, a decrease in transduction efficiency is observed across all ratios, with the most pronounced reduction occurring at a 1:100 ratio. This decrease is expected and desirable, as it indicates successful coating of the AAV, which limits viral entry into cells.

Overall, these results confirm that zwitterionic polymers alone do not form stable coatings, but when combined with CliCr, they effectively reduce transduction efficiency, demonstrating successful surface modification. Higher polymer concentrations enhance this effect, likely due to increased coating density.
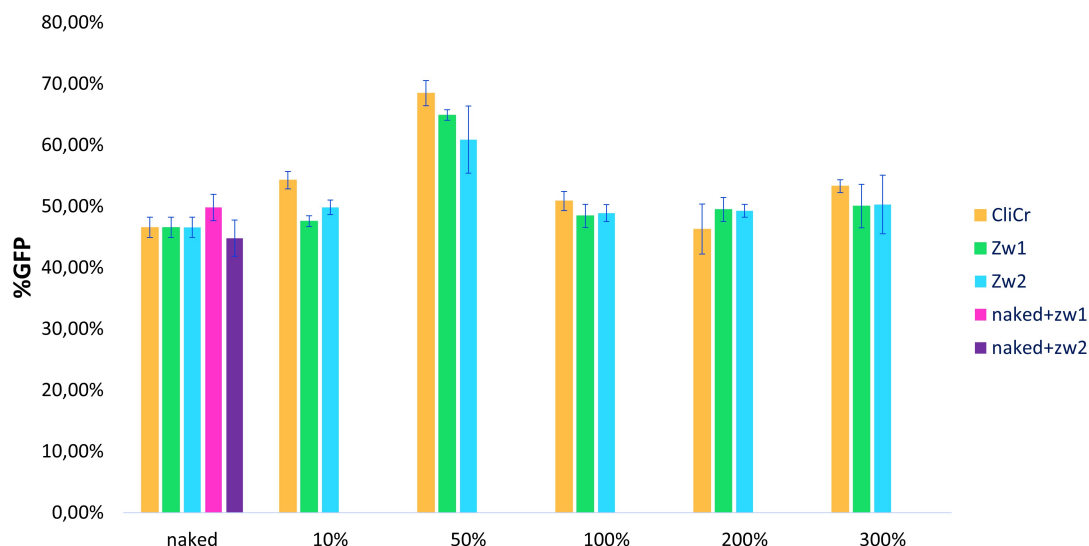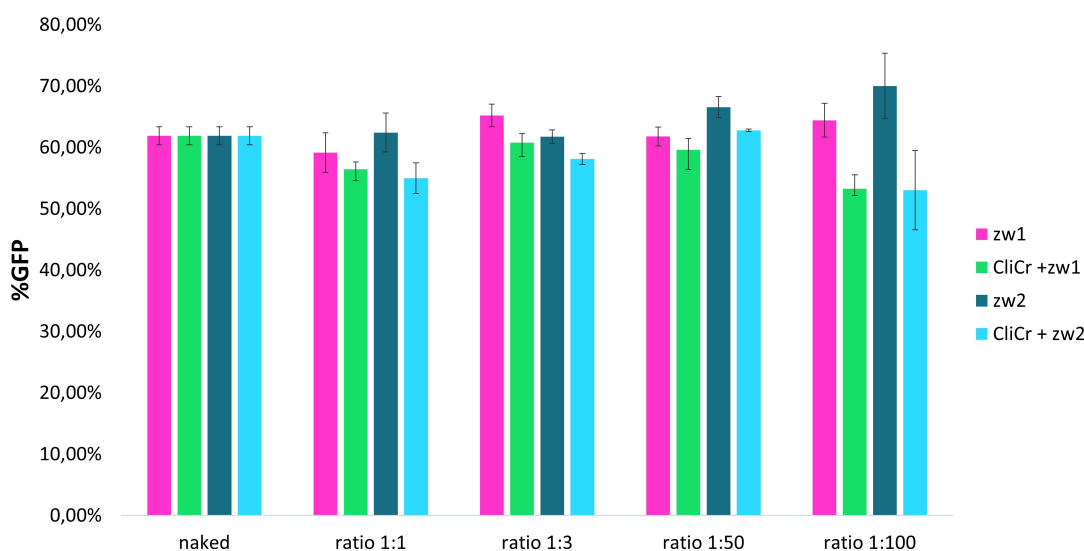

Figure 3.14: Level of expression of GFP in HeLa cell line 72 hours after transduction. The assay was performed with the AAV naked (control) and the AAV coated with different ratios (1:1, 1:3, 1:50 and 1:100) of the zwitterionic polymer 1 (zw1) in green and the zwitterionic polymer 2 (zw2) in light blue, previously bound with the 500% of the CliCr®-Osu. In pink and blue we can see zw1 and zw2 alone, as additional controls. The mean of the 3 measurements per sample, done by the Cytometer, and the Standard Deviation are plotted. The conditions used for the experiments were the same: 8000 cells per well and an MOI of 100,000.

3.3   Testing the citotoxicity of the polymeric coating

As mentioned in the transduction assay section, some samples exhibited cellular death. To better understand the cause of these undesired effects, a cell viability assay was conducted to assess the potential toxicity of the components. MTT is a colorimetric assay commonly used to assess cell metabolic activity. It is based on the reduction of a yellow water-soluble compound called MTT (3-[4,5-dimethylthiazol-2-yl]-2,5-diphenyltetrazolium bromide) by the mitochondrial enzymes of metabolically active cells into insoluble purple formazan crystals. Non-viable cells cannot perform this reduction, so the intensity of the color corresponds to the number of viable cells. All MTT assays were performed in six replicates to minimize the standard deviation.

Examining the results of the first MTT assay (**figure   3.15**), we observe that zw2 did not exhibit any signs of cytotoxicity, consistently maintaining a survival rate above 70%. In contrast, certain concentrations of CliCr and zw1 showed some degree of toxicity. Specifically, CliCr at 10%, 75%, and 100% resulted in survival rates below 10% or even negative values. This was likely due to the fact that the stock solutions of the various components were diluted in DMSO to achieve the desired concentrations, and in some samples, the amount of DMSO was too high, approaching the threshold between toxicity and non-toxicity. Additionally, the volumes used were extremely small, which could have introduced pipetting errors.

Figure 3.15: Cell viability assay of the components used for the Click reaction. The mean of the 6 measurements per sample and the Standard Deviation are plotted.

Therefore, the dilutions were redone, using HEPES buffer for the zwitterionic polymers and a lower amount of DMSO for the CliCr solutions. In the **Figure 3.16**, the second MTT assay, performed with these new dilutions and the same percentages, is shown. As seen in the plot, neither the CliCr nor the zw1 are cytotoxic, as there is more than a 60% of cell viability in all tested samples. The "CliCr 200%" condition displays a lower survival rate compared to the previous MTT assay, which is likely attributed to pipetting errors.

Figure 3.16: Cell viability assay of the components used for the Click reaction. The mean of the 6 measurements per sample and the Standard Deviation are plotted.

In parallel with the increase in reagent concentrations in the transduction experiments, an additional cell viability assay was conducted using larger volumes and concentrations of CliCr and zwitterionic polymers to assess their non-cytotoxicity at higher percentages.

As shown in the **Figure 3.17**, the survival rate consistently remains above 60%, indicating a positive outcome. However, it is evident that the survival rate for the CliCr group (represented in blue in the graph) is lower compared to the other components. This observation can be attributed to the fact that CliCr is dissolved in DMSO, that is cytotoxic at high concentrations, while the zwitterionic polymers are dissolved in Hepes buffer.
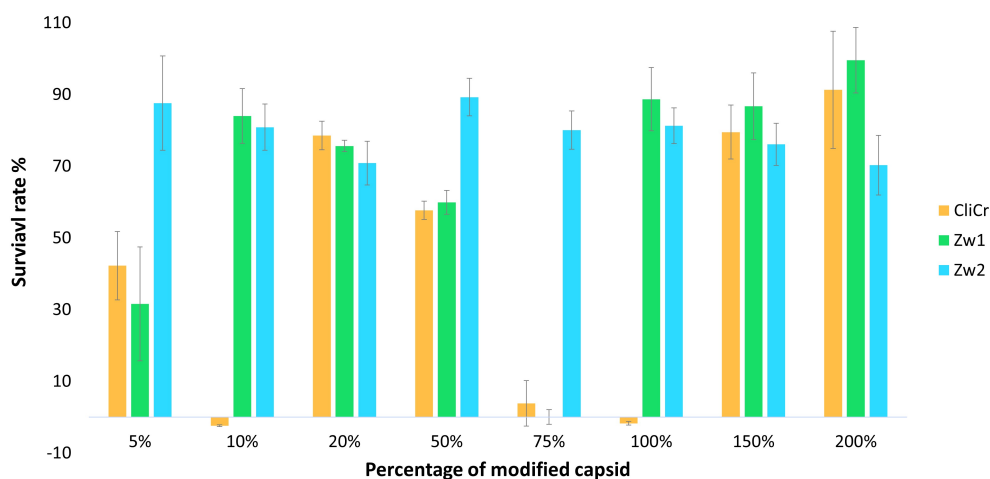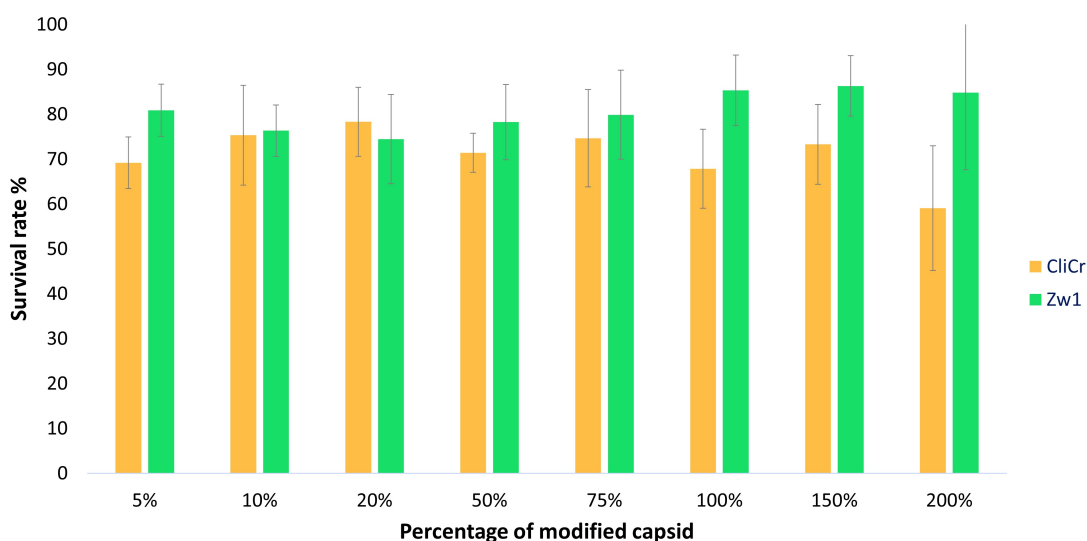
49
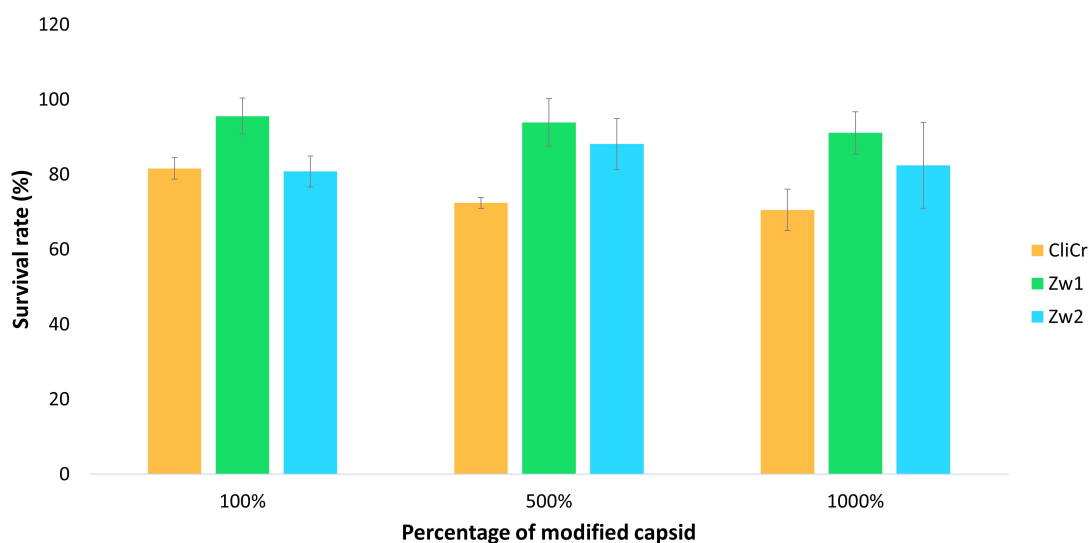
Figure 3.17: Cell viability assay of the components used for the Click reaction. The mean of the 6 measurements per sample and the Standard Deviation are plotted.

3.4 In vitro characterization of the coating process

A fluorescence analysis was conducted to confirm the occurrence of the initial step in the click reaction between the amine group and the CliCr®-Osu group. In the previous transduction experiments, it appeared that the coating was not occurring as expected. Therefore, the aim was to develop an improved protocol for coating and establish the optimal conditions for successful coating.

First, the analysis was performed with two different buffers, the HEPES buffer with pH 8,5 and the TBS buffer with pH 9,3. The goal was to determine which buffer provided the most suitable conditions for the experiment[16]. As shown in the **Figure 3.19**, the TBS buffer appeared to perform better, as it resulted in a more significant decrease in fluorescence intensity compared to the HEPES buffer. The analysis was conducted using Cy5-NHS, and as the concentration of the CliCr group increased, a corresponding decrease in fluorescence intensity was expected. Based on these results, the TBS buffer was chosen for subsequent experiments.

50
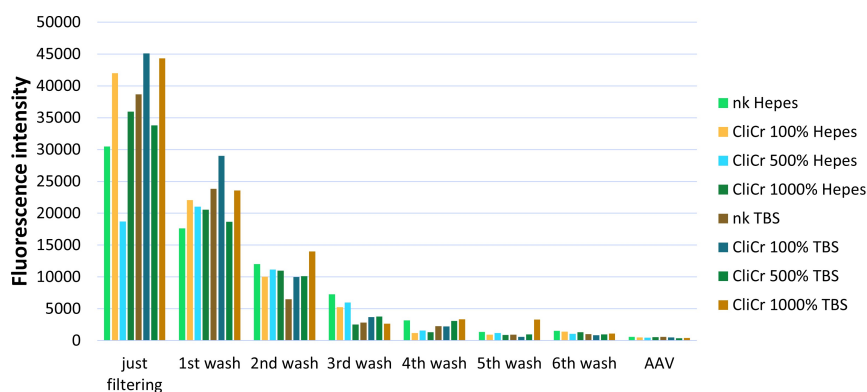
Figure 3.18: Comparison of the fluorescence intensity with different buffers
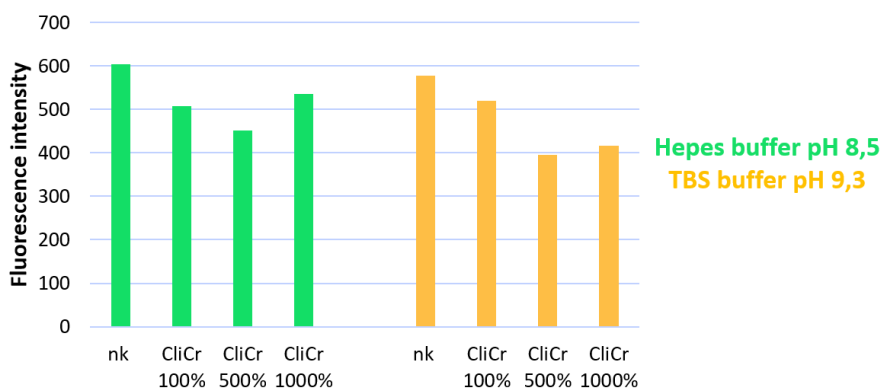
Figure 3.19: Comparison of the fluorescence intensity of the labeled AAV with different buffers

After selecting the buffer, a fluorescence analysis was performed using the Cy5-NHS molecule to indirectly determine the amount of CliCr bound to the AAV surface and, consequently, the percentage of coating achieved. Since both Cy5-NHS and CliCr bind to the same amine group on the AAV surface, we incubated the AAV first with CliCr and then with the fluorophore. Increasing the amount of CliCr should lead to a higher percentage of AAV coverage, reducing the number of free amine groups and, as a result, decreasing the amount of fluorophore bound to the AAV. The analyzed percentages were 500%, 1000%, 10000%, and 100000%. We deliberately exaggerated the amount of CliCr to observe if there was a measurable change in behavior with the increase of the molecule to very high levels.

As illustrated in the **Figure 3.20b**, no clear trend is observed with an increase in the percentage of the CliCr-Osu group. The fluorescence intensity appears to

decrease between the naked AAV and CliCr at 500%, remains relatively constant between 500% and 1000%, and then increases beyond 1000%. This behavior could be attributed to the potential inefficiency of the Amicon filters, which may have failed to wash away some fluorescent molecules, leaving them in the AAV solution.

(a)

(b)

Figure 3.20: Fluorescence analysis after the labeling with the Cy5-NHS : (a) Fluorescence intensity in the different washes; (b) Fluorescence intensity of the labeled AAV

The same experiment was conducted under the same conditions, but with a different fluorophore. The objective remained the same, but the expected result was the opposite. This is because Cy3-N3 binds to the other end of the CliCr group, so its binding should increase in proportion to the amount of CliCr. As shown in **Figure 3.21b** a distinct trend is observed when increasing the percentage

of the CliCr group. Specifically, the Cy3-NHS fluorescence intensity exhibits a proportional increase as the percentage of the CliCr group rises. In the case of the naked AAV, the fluorescence intensity is approximately 10. Although this value is not exactly zero, it is notably close to the hypothetical result that was expected, further supporting the reliability of the observed trend in this experiment.
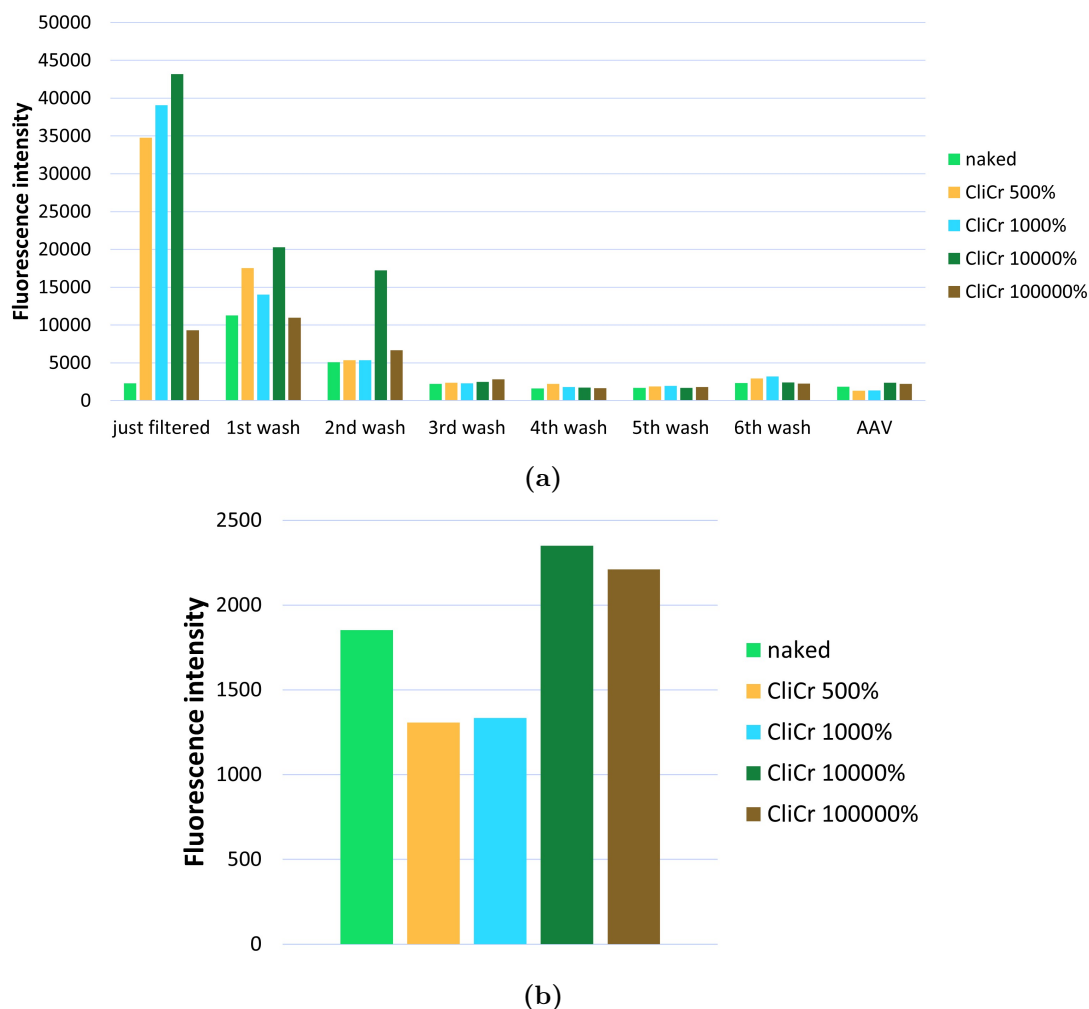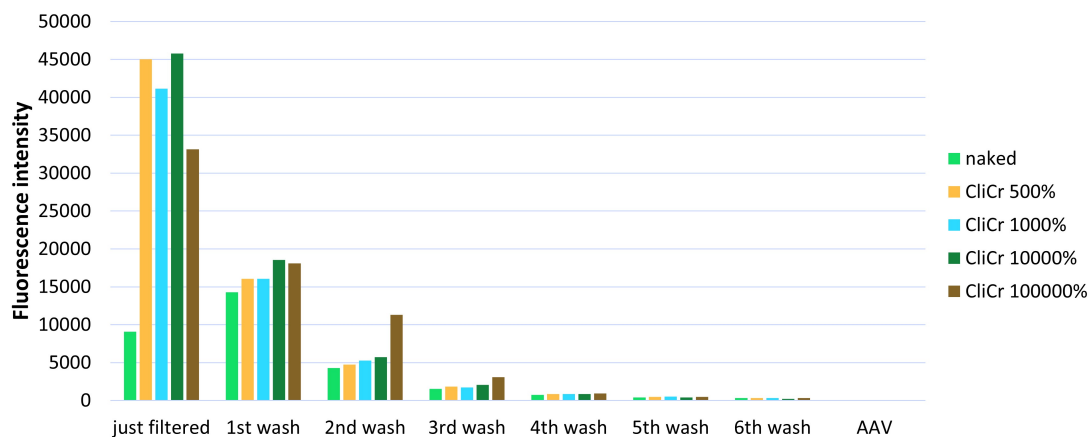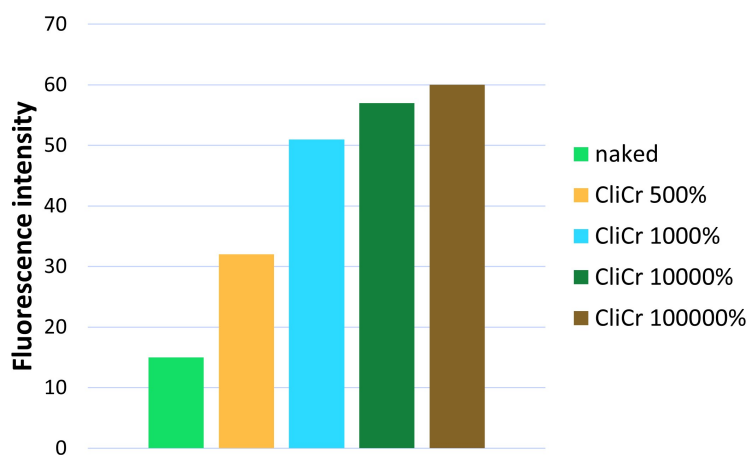

(a)

(b)

Figure 3.21: Fluorescence analysis after the labeling with the Cy3-N3 : (a) Fluorescence intensity in the different washes; (b) Fluorescence intensity of the labeled AAVs

The same experiment was performed for both fluorophores, with the same conditions. However, the results indicate that the procedure appears to work more effectively for Cy3-N3. This difference could potentially be attributed to the higher molecular weight of Cy5, which may act as a barrier or "plug" on the membrane of the filters. Consequently, this could prevent the excess Cy5 fluorophore from passing through the filters effectively.

In summary, the in vitro characterization of the coating process and transduction studies provided valuable insights into the efficiency and stability of the Click Chemistry coating strategy. While these analyses confirmed the successful initiation of the click chemistry reaction, they also highlighted inconsistencies in coating efficiency, likely due to experimental variability or buffer selection. These findings underscored the need for further optimization of the coating protocol.
The next step was to compare these results with the previously tested strategies by the GEMAT group, electrostatic interactions and covalent coating, to assess the potential superiority of the Click Chemistry approach.

3.5 Comparison of the strategies

In this work, three distinct strategies were explored to coat AAVs: electrostatic, covalent and click chemistry. The aim was to evaluate the effectiveness of these coatings in terms of both stability and their ability to facilitate cellular entry, which is essential for efficient gene delivery.

3.5.1 Coating characterization

Zeta potential analysis was first conducted to measure the surface charge and stability of the coated AAV particles. The zeta potential measurements, as shown in **Figure 3.22**, demonstrate the surface charge characteristics of the AAV under various conditions. The first column represents the zeta potential of the naked AAV, which exhibits a negative value, as expected due to the natural surface charge of the viral capsid. Upon coating with CliCr at 1000% (2nd column) and CliCr 1000% and zwitterionic polymer(3rd column), there is an observable increase in zeta potential. This suggests a partial neutralization of the capsid's negative charge, indicating the successful attachment of the zwitterionic polymer to the AAV via the CliCr compound. The last three columns correspond to different coating strategies: covalent (C6CR3 NHS), electrostatic (C6CR3) and the new synthetized polymer (C6N3). These coatings result in a positive zeta potential, confirming a successful charge inversion of the capsid surface. This is consistent with the expected outcomes for these coatings, as the positive charge suggests an effective modification of the viral surface.
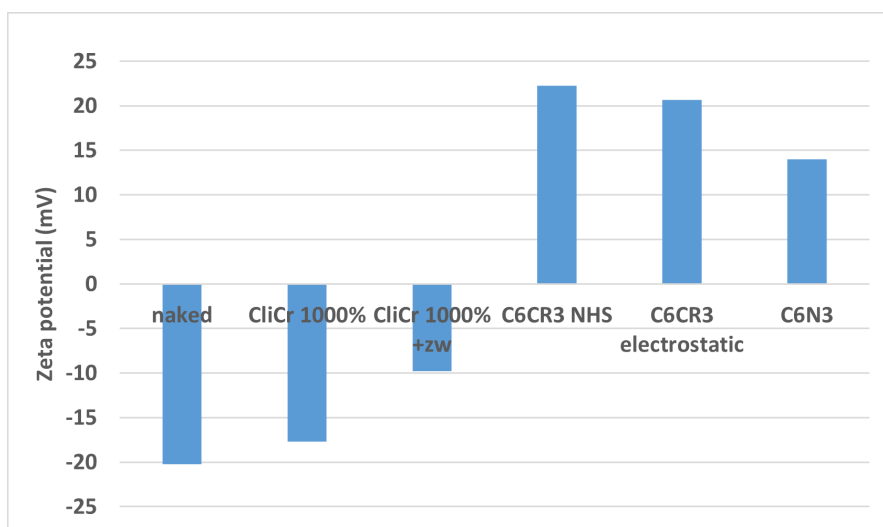
Figure 3.22: Comparison of the zeta-potential with different strategies

3.5.2 Coating effectiveness

To evaluate the efficiency of cellular entry for both uncoated (naked) and coated AAV particles, a transduction study was performed. The study aimed to compare the internalization of the viral vectors modified through the three distinct coating strategies.

We analyzed coatings with two different percentages of CliCr, 300% and 500%, rather than the highest percentages tested in the fluorescence analysis (see Section 3.4). Although the highest percentage of CliCr (100.000%) appeared to yield better results with Cy3, the analysis with Cy5 did not show the same improvement. In fact, Cy5 seemed to work slightly better with the 500% condition. Additionally, the 10000% and 100000% percentages were exaggerated to observe the behavior at very high levels, and were not intended for use in subsequent experiments.

As we can see in the **Figure 3.23**, the electrostatic coating appears to be the least stable. In fact, the %GFP value is similar to that of the naked AAV, possibly due to the detachment of the coating. In contrast, the covalent polymer coating enhances cellular entry.

Regarding the click chemistry strategy, the results are shown in yellow and green. With CliCr 300%, no clear trend is observed, suggesting that the amount of CliCr may not be sufficient to effectively coat the AAV. However, with CliCr 500%, a decrease in cellular entry is observed when zwitterionic polymers are added, particularly at a 1:500 ratio. Among the zwitterionic polymers tested, polymer 2 appears to be the most promising, as previously noted, potentially due to its higher molecular weight.
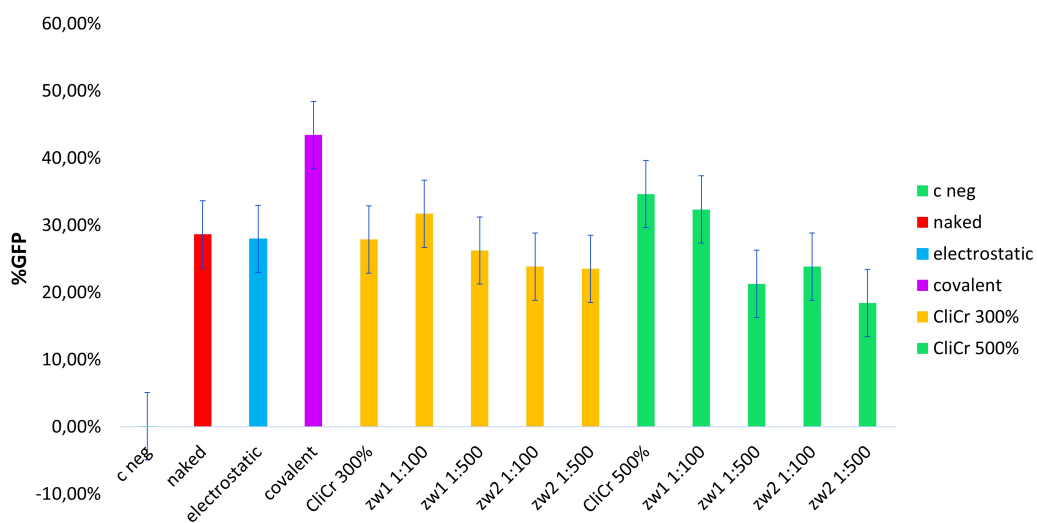
Figure 3.23: Level of expression of GFP in HeLa cell line 72 hours after transduction with 8000 cells/well and MOI 100000. The assay was performed with the AAV naked (control) and coated with different percentages of the zwitterionic polymer 1 (zw1) and zwitterionic polymer 2 (zw2) bound also with different percentages of CliCr®-Osu (300% and 500%). The percentages used are not the same for the CliCr molecule and the zwitterionic polymers (1:100 and 1:500 molar ratios). In yellow we can see the CliCr 300% and in green the CliCr 500%. In blue there is the electrostatic coating and in purple the covalent one. The mean of the 3 measurements per sample, done by the Cytometer, and the Standard Deviation are plotted.

3.6 Transduction of C2C12 with peptides

Another approach was to conduct experiments using muscle-specific cell lines, such as the C2C12 cell line. Also if HeLa cells are a suitable model for these experiments and allow for the assessment of GFP expression via the CMV promoter, they do not represent the target cell type for the therapy.

Therefore, testing different coatings on the C2C12 cell line would be a valuable strategy for the analysis. However, for the coated vector to enter the C2C12 cells, a signaling peptide, such as the AAVMYO peptide, must be incorporated into its structure. This peptide would specifically target muscle cells and enhance their uptake. The C6-N3 pBAE and a zwitterionic polymer binded to AAVMYO were used for the transduction experiments.

This approach also served to assess in another way the efficiency of the coating via click chemistry, as naked AAV has low transduction efficiency in C2C12 cells. If we observe an increase in AAV entry, it would indicate that the strategy is working effectively.

The transduction was performed on AAVs naked and coated with the Click Chemistry strategy with more polymers:

- Zwitterionic polymer 2

- Zwitterionic polymer binded with the peptide (pep2-zw)

- combination of the previous two in varying percentages

- C6N3 pBAE binded with the peptide

In **Figure 3.24**, the GFP expression in C2C12 cells is shown 48 hours after transduction, providing insights into the efficiency of two of the coatings: with the C6N3 polymer and with the peptide, both binded to the AAV through the CliCr molecule.

As expected, the GFP expression in cells treated with naked AAVs is relatively low, confirming the limited transduction efficiency of unmodified vectors in the C2C12 (**Figure 3.24a** and **Figure 3.24b**).

When a coating is applied, a significant increase in GFP expression is observed, indicating an improved transduction process. In particular, the condition in which AAVs were coated only with the peptide shows a remarkably high GFP expression compared to the naked AAVs (**Figure 3.24e** and **Figure 3.24f**), demonstrating the strong impact of the peptide in enhancing cellular entry.

Additionally, the images show the GFP expression in cells transduced with AAVs coated using the newly synthesized C6N3 pBAE polymer linked with the peptide (**Figure 3.24c** and **Figure 3.24d**). The increased fluorescence signal in this condition confirms the successful synthesis of the polymer and validates

the coating strategy. These results support the hypothesis that both the peptide and the polymer contribute to improving AAV transduction efficiency and so the targeting.
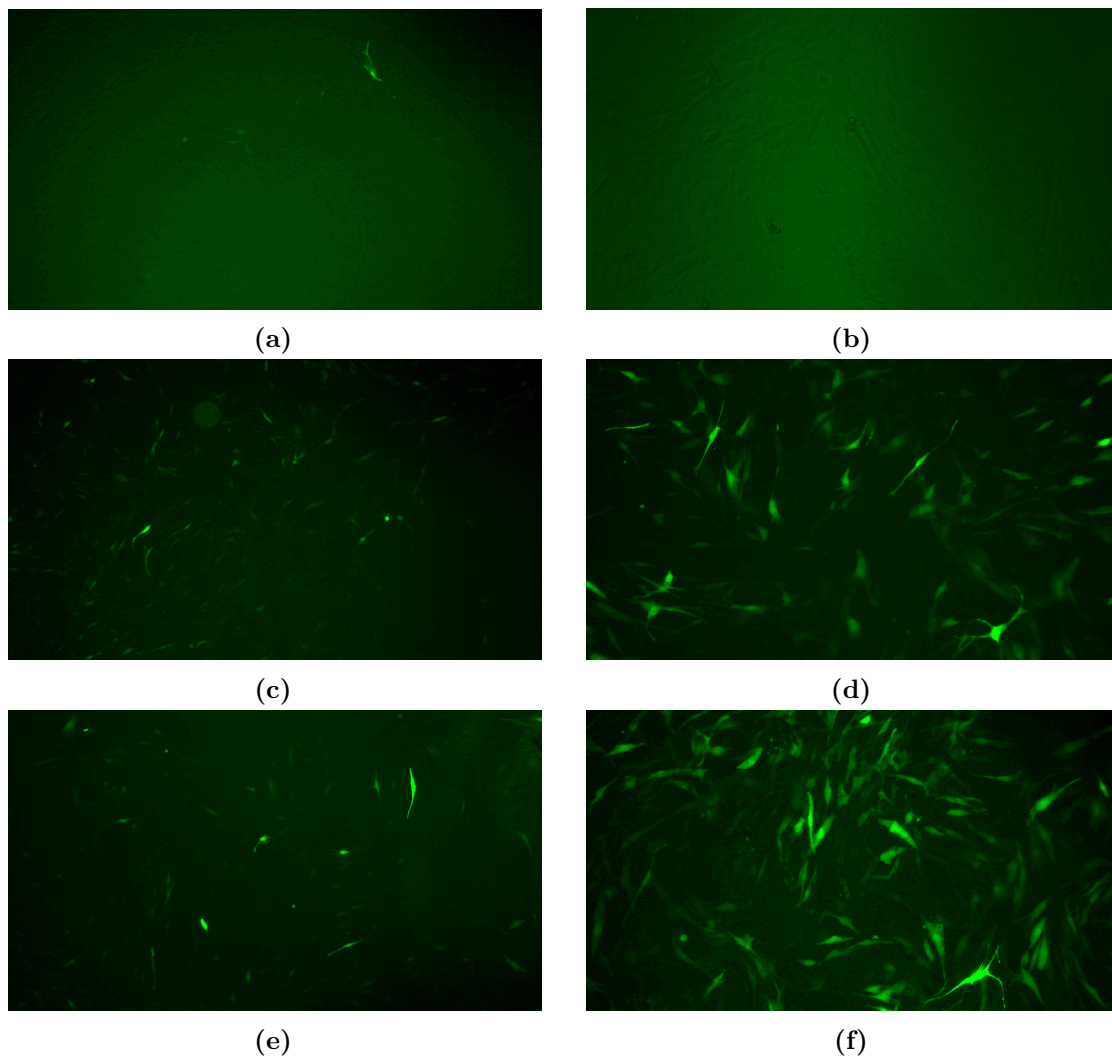
Figure 3.24: Fluorescence microscopy images captured 48 hours after transduction, showing the expression of the transgene in different experimental conditions. The three images at the left were taken at 5× magnification, while the other three were taken at 10× magnification. Each condition includes (a,b) naked AAV, (c,d) AAV coated with the C6N3 pBAE polymer, and (e,f) AAV coated only with the peptide. Differences in fluorescence intensity and distribution reflect the impact of the coating strategies on transduction efficiency.

As expected, the negative control (C neg) showed negligible GFP expression, while the naked AAV (nk, red) exhibited a low level of transduction, serving as the baseline for comparison. See **Figure 3.25**.

When AAV was coated with zwitterionic polymer 2 (zw2), an increase in transduction efficiency was observed compared to the naked AAV. Further modifications were introduced by incorporating different percentages (1%, 5%, 10%, 50%, 75% and 100%) of a zwitterionic polymer conjugated to a peptide (pep2-zw, green bars). A clear trend was observed: as the percentage of pep2-zw increased, transduction efficiency also improved, reaching its highest values at 75% and 100% modifications.

AAV coated only with the peptide (CliCr + peptide, dark green) showed comparable or slightly improved transduction levels relative to the highest pep2-zw percentages, indicating that the peptide itself may enhance viral entry.

Finally, the newly synthesized polymer C6N3 pBAE (blue) resulted in a lower %GFP compared to the highest values obtained with pep2-zw, suggesting that while this polymer allows AAV entry, its efficiency is reduced compared to the peptide-modified zwitterionic polymers.
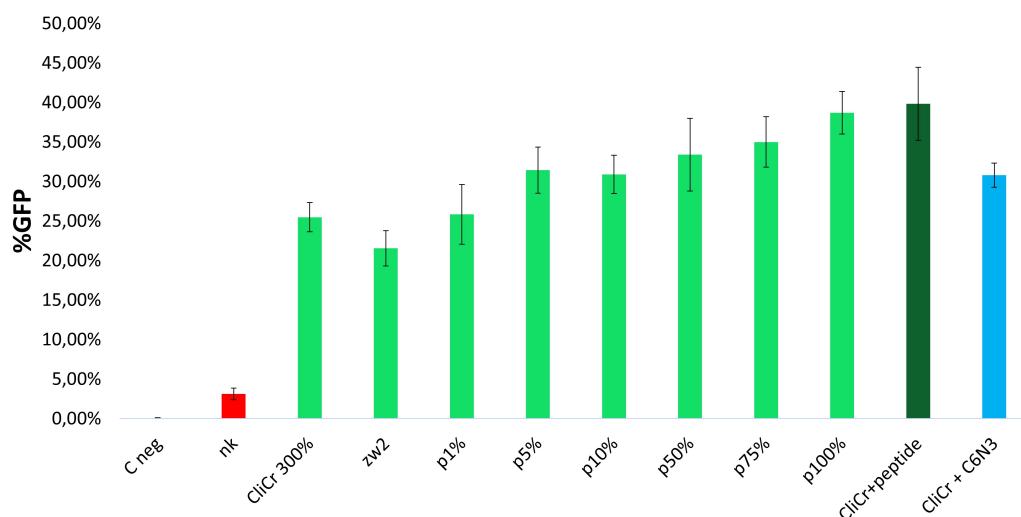
Figure 3.25: Level of expression of GFP in C2C12 cell line 72 hours after transduction with 15000 cells/well and MOI 100000. The assay was performed using naked AAV (red), AAV coated with zwitterionic polymer 2 (zw2) combined with varying percentages (0%, 1%, 5%, 10%, 50%, 75%, and 100%) of a zwitterionic polymer linked to a peptide (pep2-zw) (green), AAV coated only with the peptide (dark green), and AAV coated with the newly synthesized C6N3 pBAE polymer (blue). The mean of the 3 measurements per sample, done by the Cytometer, and the Standard Deviation are plotted.

Chapter 4

Conclusions

From all these studies, the following conclusions can be drawn:

- The synthesis of the polymer C6-N3 pBAE worked, as confirmed by the IR and NMR analysis

- The C6-N3 has a semicrystalline nature and is better classified as an oligomer rather than a true polymer.

- The Zeta-potential analysis does not demonstrate if the zwitterionic polymer binds to the CliCr molecule

- The click chemistry reaction seem to need the various component in excess: with a low amount of CliCr®-Osu the reaction seems to no occur

- The CliCr®-Osu and the zwitterionic polymers seem to be non-cytotoxic also in higher amount

- The fluorescence analysis with the Cy3-N3 confirmed that the first reaction between the AAVs and the CliCr®-Osu occured, but more studies should be carried out to understand if occurs the second reaction between the CliCr®-Osu and the zwitterionic polymers

- With the C2C12, the transduction efficiency seems to increase with the polymer linked with the peptide (AAVMYO), so there is a targeting of the treatment

Bibliography

[1] X. Zhou et al. «Adeno-Associated Virus Engineering and Load Strategy for Tropism Modification, Immune Evasion and Enhanced Transgene Expression». In: *International Journal of Nanomedicine* 19 (2024), pp. 7691–7708. DOI: 10.2147/IJN.S459905.

[2] National Institute of Neurological Disorders and Stroke National Institutes of Health. «Muscular distrophy». In: *NIH Publication* 13-77 (2023).

[3] Quan Q. Gao and Elizabeth M. McNally. «The Dystrophin Complex: Structure, Function, and Implications for Therapy». In: *Comprehensive Physiology* 5 (2015), pp. 1223–1239. DOI: 10.1002/cphy.c140048.

[4] Damon R. Asher et al. «Clinical Development on the Frontier: Gene Therapy for Duchenne Muscular Dystrophy». In: *Expert Opinion on Biological Therapy* 20 (2020), pp. 263–274. DOI: 10.1080/14712598.2020.1725469.

[5] A. Bez Batti Angulski et al. «Duchenne Muscular Dystrophy: Disease Mechanism and Therapeutic Strategies». In: *Frontiers in Physiology* 14 (2023). DOI: 10.3389/fphys.2023.1183101.

[6] Mde L. Beytía, J. Vry, and J. Kirschner. «Drug Treatment of Duchenne Muscular Dystrophy: Available Evidence and Perspectives». In: *Acta Myologica: Myopathies and Cardiomyopathies: Official Journal of the Mediterranean Society of Myology* 31 (2012), pp. 4–8.

[7] *FDA grants accelerated approval to first drug for Duchenne muscular dystrophy.* 2016. URL: https://www.fda.gov/news-events/press-announcements/fda-grants-accelerated-approval-first-drug-duchenne-muscular-dystrophy.

[8] Young Jik Kwon Margaret L. Lugin Rebecca T. Lee. «Synthetically Engineered Adeno-Associated Virus for Efficient, Safe, and Versatile Gene Therapy Applications». In: *ACS Nano* 14 (2020), pp. 14262–14283. DOI: 10.1021/acsnano.0c03850.

[9] Assumpcio Bosch and Miguel Chillon. «Gene Therapy Approaches in Central Nervous System Regenerative Medicine». In: *Handbook of Innovations in Central Nervous System Regenerative Medicine* 10 (2020). DOI: `https://doi.org/10.1016/B978-0-12-818084-6.00010-6`.

[10] Z. Zhao, A. C. Anselmo, and S. Mitragotri. «Viral Vector-Based Gene Therapies in the Clinic». In: *Bioengineering Translational Medicine* 7 (2021). DOI: `10.1002/btm2.10258`.

[11] Y. H. Chen, M. S. Keiser, and B. L. Davidson. «Viral Vectors for Gene Transfer». In: *Current Protocols in Mouse Biology* 8 (2018). DOI: `10.1002/cpmo.58`.

[12] W. C. Russell. «Update on Adenovirus and Its Vectors». In: *Journal of General Virology* 81 (2000), pp. 2573–2604. DOI: `https://doi.org/10.1099/0022-1317-81-11-2573`.

[13] Hanna J. Wagner, Wilfried Weber, and Martin Fussenegger. «Synthetic Biology: Emerging Concepts to Design and Advance Adeno-Associated Viral Vectors for Gene Therapy». In: *Advanced Science* 8 (2021), e2004018. DOI: `10.1002/advs.202004018`.

[14] M. Guerra-Rebollo, M. Stampa, and MÁ. et al. Lázaro. «Electrostatic Coating of Viral Particles for Gene Delivery Applications in Muscular Dystrophies: Influence of Size on Stability and Antibody Protection». In: *Journal of Neuromuscular Diseases* 8 (2021), pp. 815–825. DOI: `10.3233/JND-210662`.

[15] Dongsheng Duan. «Systemic AAV Micro-Dystrophin Gene Therapy for Duchenne Muscular Dystrophy». In: *Molecular Therapy* 26 (2018). DOI: `https://doi.org/10.1016/j.ymthe.2018.07.011`.

[16] Anh K. Lam et al. «Chemical Modifications of the Capsid for Redirecting and Improving the Efficacy of Adeno-Associated Virus Vectors». In: *Human Gene Therapy* 32 (2021), pp. 1433–1438. DOI: `10.1089/hum.2021.124`.

[17] Yong Liu et al. «Poly(β-Amino Esters): Synthesis, Formulations, and Their Biomedical Applications». In: *Advanced Healthcare Materials* 8 (2018), e1801359. DOI: `DOI:10.1002/adhm.201801359`.

[18] Jiayu et al. Zhang. «Poly(β-Amino Ester)s-Based Nanovehicles: Structural Regulation and Gene Delivery». In: *Molecular Therapy Nucleic Acids* 32 (2023), pp. 568–581. DOI: `https://doi.org/10.1016/j.omtn.2023.04.019`.

[19] N. Segovia et al. «Oligopeptide-Terminated Poly(β-Amino Ester)s for Highly Efficient Gene Delivery and Intracellular Localization». In: *Acta Biomaterialia* 76 (2018). DOI: `https://doi.org/10.1016/j.actbio.2018.06.011`.

[20] C. Fornaguera et al. «In Vivo Retargeting of Poly(beta aminoester) (OM-PBAE) Nanoparticles is Influenced by Protein Corona». In: *Advanced healthcare materials* 8 (2019), e1900849. DOI: `10.1002/adhm.201900849`.

[21] C. Fornaguera et al. «mRNA Delivery System for Targeting Antigen-Presenting Cells In Vivo». In: *Advanced healthcare materials* 7 (2018), e1800335. DOI: `doi:10.1002/adhm.201800335`.

[22] Ladd et al. «Zwitterionic Polymers Exhibiting High Resistance to Nonspecific Protein Adsorption from Human Serum and Plasma». In: *Biomacromolecules* 9 (2008), pp. 1357–1361. DOI: `10.1021/bm701301s`.

[23] Keyu Qu et al. «Structures, properties, and applications of zwitterionic polymers». In: *ChemPhysMater* 1 (2022), pp. 294–309. DOI: `https://doi.org/10.1016/j.chphma.2022.04.003`.

[24] O. Schussler et al. «Possible Treatment of Myocardial Infarct Based on Tissue Engineering Using a Cellularized Solid Collagen Scaffold Functionalized with Arg-Gly-Asp (RGD) Peptide». In: *International Journal of Molecular Sciences* 22.22 (2021), p. 12563. DOI: `10.3390/ijms222212563`.

[25] M. Tabebordbar et al. «Directed Evolution of a Family of AAV Capsid Variants Enabling Potent Muscle-Directed Gene Delivery Across Species». In: *Cell* 184 (2021), pp. 4919–4938. DOI: `10.1016/j.cell.2021.08.028`.

[26] Nicolò Zuin Fantoni, Afaf H. El-Sagheer, and Tom Brown. «A Hitchhiker's Guide to Click-Chemistry with Nucleic Acids». In: *Chemical Reviews* 121 (2021), pp. 7122–7154. DOI: `10.1021/acs.chemrev.0c00928`.

[27] John E. Moses and Adam D. Moorhouse. «The Growing Applications of Click Chemistry». In: *Chemical Society Reviews* 36 (2007), pp. 1249–1262. DOI: `10.1039/b613014n`.

[28] Vinod K. Tiwari et al. *Click Chemistry*. Springer, 2024.

[29] A. C. et al. Panda. «RNA-Binding Protein AUF1 Promotes Myogenesis by Regulating MEF2C Expression Levels». In: *Molecular and Cellular Biology* 34.16 (2014), pp. 3106–3119. DOI: `10.1128/MCB.00423-14`.